https://doi.org/10.5194/gmd-2021-327
Preprint. Discussion started: 25 October 2021

Geoscientific Model Development Discussions

Ocean biogeochemistry in the Canadian Earth System Model version 5.0.3: CanESM5 and CanESM5-CanOE

James R. Christian[1,2], Kenneth L. Denman[2,3], Hakase Hayashida[3,4], Amber M. Holdsworth[1], Warren G. Lee[2], Olivier G.J. Riche[3,5], Andrew E. Shao[2,3], Nadja Steiner[1,2], and Neil C. Swart[2]

1 Fisheries and Oceans Canada, Sidney, BC, Canada
2 Canadian Centre for Climate Modelling and Analysis, Victoria, BC, Canada
3 School of Earth and Ocean Sciences, University of Victoria, Victoria, BC, Canada
4 now at the Institute for Marine and Antarctic Studies, University of Tasmania, Hobart, Tasmania, Australia
5 now at Fisheries and Oceans Canada, Mont Joli, Québec, Canada

Correspondence to: James Christian (jim.christian@ec.gc.ca)

https://doi.org/10.5194/gmd-2021-327
Preprint. Discussion started: 25 October 2021

Geoscientific Model Development Discussions

Abstract. The ocean biogeochemistry components of the Canadian Earth System Model v. 5 are presented and compared to observations and other models. CanESM5 employs the same biogeochemistry module as CanESM2 whereas CanESM5-CanOE ("Canadian Ocean Ecosystem model") is a new, more complex biogeochemistry module developed for CMIP6, with multiple food chains, flexible phytoplankton elemental ratios, and a prognostic iron cycle. This new model is described in detail and the outputs compared to CanESM5 and CanESM2, as well as to observations and other CMIP6 models. Both CanESM5 models show gains in skill relative to CanESM2, which are attributed primarily to improvements in ocean circulation. CanESM5-CanOE shows improved skill relative to CanESM5 in some areas. CanESM5-CanOE includes a prognostic iron cycle, and maintains high nutrient / low chlorophyll conditions in the expected regions (in CanESM2 and CanESM5, iron limitation is specified as a temporally static 'mask'). Surface nitrate concentrations are biased low in the subarctic Pacific and equatorial Pacific, and high in the Southern Ocean. Export production in CanESM5-CanOE is among the lowest for CMIP6 models; in CanESM5 it is among the highest, but shows the most rapid decline after about 1980. CanESM5-CanOE has relatively low concentrations of zooplankton and detritus relative to phytoplankton, and a high and relatively constant living phytoplankton fraction of total particulate organic matter. In most regions, large and small phytoplankton show decoupled seasonal cycles with greater abundance of large phytoplankton in the productive seasons. Cumulative ocean uptake of anthropogenic carbon dioxide through 2014 is lower in both CanESM5 models than in observation-based estimates or the model ensemble mean, and is lower in CanESM5-CanOE (122 PgC) than in CanESM5 (132 PgC).

https://doi.org/10.5194/gmd-2021-327
Preprint. Discussion started: 25 October 2021

Geoscientific Model Development Discussions

1. **Introduction**

The Canadian Centre for Climate Modelling and Analysis has been developing coupled models with an interactive carbon cycle for more than a decade (Arora et al., 2009; 2011; Christian et al., 2010). CanESM5 (Swart et al., 2019a) is an updated version of CanESM2 (Arora et al., 2011), with an entirely new ocean and an atmosphere with the same T63 horizontal resolution and important improvements in atmospheric physics. The CanESM5 ocean is based on the Nucleus for European Modelling of the Ocean (NEMO) system version 3.4. The ocean biogeochemistry modules were developed in-house, although parameterizations for some processes were adapted from the native PISCES biogeochemistry model (Aumont et al., 2015). CanESM5 uses the same biogeochemistry model as CanESM1 and CanESM2, the Canadian Model of Ocean Carbon (CMOC; Zahariev et al., 2008), adapted for use within NEMO. An additional model was developed for CMIP6, called the Canadian Ocean Ecosystem model (CanOE). The biological components of CanOE are of substantially greater complexity, including multiple food chains, flexible phytoplankton elemental ratios, and a prognostic iron (Fe) cycle. Carbon chemistry, gas exchange and solubility of carbon dioxide (CO_2) and oxygen are identical between the two and follow the protocols specified by the Ocean Model Intercomparison Project - Biogeochemistry (OMIP-BGC) (Orr et al., 2017). The two coupled models are known as CanESM5 and CanESM5-CanOE, respectively. There are no feedbacks between biology and the physical ocean model, so the physical climate of CanESM5 and CanESM5-CanOE is identical in experiments with prescribed atmospheric CO_2 concentration.

The reasons for developing both models are, firstly, to evaluate the effect of changes in ocean

https://doi.org/10.5194/gmd-2021-327
Preprint. Discussion started: 25 October 2021


Geoscientific Model Development Discussions

circulation between CanESM2 and CanESM5 on ocean biogeochemistry by running the new climate model with the same ocean biogeochemistry, and secondly because CanOE is substantially more expensive computationally (19 tracers vs 7). Having CMOC as an option allowed us to run many CMIP6 experiments with CanESM5 only, as ocean biogeochemistry is not central to their purpose. Many additional tracers requested by OMIP-BGC including abiotic and natural dissolved inorganic carbon (DIC), DI^{14}C, CFCs and SF_6 (see Orr et al.,2017) were run only in CanESM5, since adding these tracers on top of the larger set of biological components in CanOE would have been prohibitively expensive. The CMIP6 experiments published for CanESM5-CanOE are listed in Supplementary Table S1.

CMOC is a nutrient-phytoplankton-zooplankton-detritus (NPZD) model with highly parameterized representations of phytoplankton Fe limitation, dinitrogen (N_2) fixation and denitrification, and calcification and calcite dissolution (Zahariev et al., 2008). In CanESM1 and CanESM2, CMOC did not include oxygen. In CanESM5, CMOC now includes oxygen as a purely 'downstream' tracer that does not affect other biogeochemical processes, whereas in CanOE denitrification is prognostic and dependent on the concentration of oxygen. Among the less satisfactory aspects of CMOC biogeochemistry are, firstly, that Fe limitation is specified as a static 'mask' that does not change with climate (being calculated from the present-day climatological distribution of nitrate), and secondly, that denitrification is parameterized so that nitrogen (N) is conserved within each vertical column, i.e., collocated with N_2 fixation in tropical and subtropical open-ocean regions (Zahariev et al., 2008; Riche and Christian, 2018). This latter simplification produced excessive accumulations of nitrate in Eastern Boundary Current regions where most denitrification actually occurs. CMOC also has a tendency to produce rather stark

https://doi.org/10.5194/gmd-2021-327
Preprint. Discussion started: 25 October 2021


Geoscientific Model Development Discussions

extremes of high and low primary and export production (Zahariev et al., 2008), a well-known problem of NPZD models (Armstrong, 1994; Friedrichs et al., 2007). Our intent in developing CanOE was to alleviate, or at least reduce, these biases, by including multiple food chains, a prognostic Fe cycle, and prognostic denitrification. Dinitrogen fixation is still parameterized, but the CanOE parameterization includes Fe limitation, whereas in CMOC N_2 fixation tends to grow without bound in a warming ocean as there is no P or Fe limitation (Riche and Christian, 2018). Calcification is represented by a prognostic detrital calcite pool with its own sinking rate (distinct from that of organic detritus), and calcite burial depends on the saturation state. In CMOC calcification is parameterized by a temperature dependent "rain ratio" and 100% burial of calcite that reaches the seafloor is assumed.

In this paper we present a detailed model description for CanOE and an evaluation of both CanESM5 and CanESM5-CanOE relative to observational data products and other available models. CMOC has been well described previously (Zahariev et al., 2008) and the details are not reiterated here. In some cases, CanESM2 results are also shown to illustrate which differences in the model solutions arise largely from the evolution of the physical ocean model, and which are specifically associated with different representations of biogeochemistry.

2. Model Description

The NEMO system is a publicly available archive of codes based on the OPA (Océan PArallelisé) ocean model (Madec and Imbard, 1996; Guilyardi and Madec, 1997). It comes with two options for biogeochemistry: PISCES (Pelagic Interactions Scheme for Carbon and

https://doi.org/10.5194/gmd-2021-327
Preprint. Discussion started: 25 October 2021


Geoscientific Model Development Discussions

Ecosystem Studies) and LOBSTER (LODyC Ocean Biogeochemical System for Ecosystem and Resources). CanOE and the NEMO implementation of CMOC are built around the basic code structure of PISCES within the Tracers in Ocean Paradigm (TOP) module, using NEMO v3.4.1, but have also been implemented in NEMO 3.6 for regional downscaling applications (Holdsworth et al., 2021).

The biology, carbon chemistry, gas exchange and light attenuation components have all been modified to various degrees. In a few cases PISCES parameterizations, or slightly modified versions thereof, were adopted. CanOE uses PISCES three-band light attenuation while NEMO-CMOC uses broadband attenuation of photosynthetically active radiation (PAR) for consistency with the published version of CMOC. Carbon chemistry was modified to be consistent with the Best Practices Guide (Dickson et al., 2007) and the OMIP-BGC data request (Orr et al., 2017). All calculations are done on the total scale and the recommended formulae for the equilibrium constants are employed. The PISCES conventions for convergence of carbon chemistry calculations were retained, the greater number of iterations in the surface layer offering greater accuracy in calculating pCO_2 and gas exchange. In subsurface layers (where the only function of the carbon chemistry is to calculate burial of calcite in the sediments) the number of iterations is fixed at five. CanESM5 uses the same carbon chemistry but does not solve the carbon chemistry equations in the subsurface layers.

The CanOE biology model is a substantially new model based on the cellular regulation model of Geider et al. (1998). There are two phytoplankton functional groups, and each group has four state variables: C, N, Fe and chlorophyll. Photosynthesis is decoupled from cell production and

https://doi.org/10.5194/gmd-2021-327
Preprint. Discussion started: 25 October 2021


Geoscientific Model Development Discussions

photosynthetic rate is a function of the cell's internal N and Fe quotas. Each functional group has a specified minimum and maximum N quota and Fe quota, and nutrient uptake ceases when the maximal cell quota is reached. Chlorophyll synthesis is a function of N uptake and increases at low irradiance. Model parameters and their values are listed in Table 1. A schematic of the model is shown in Figure 1.

2.1 Photosynthesis and Phytoplankton Growth

For simplicity and clarity, the equations are shown here for a single phytoplankton species, and do not differ structurally for small and large phytoplankton. Some parameter values differ for the two phytoplankton groups; all parameter values are listed in Table 1.

Temperature dependence of photosynthetic activity is expressed by the Arrhenius equation

$$T_f = \exp\left(-\frac{E_{ap}}{R}\left(\frac{1}{T} - \frac{1}{T_{\text{ref}}}\right)\right) \quad (1)$$

where E_{ap} is an enzyme activation energy that corresponds approximately to that of RuBisCo (cf. Raven and Geider 1988), R is the gas constant (8.314 J mol^{-1} K^{-1}), and temperature T and reference temperature T_{ref} are in Kelvin. Maximal rates of nutrient (either N or Fe, but generically referred to here with the superscript X) uptake are given by

$$V_{max}^{X} = V_{ref}^{X} T_f \left(\frac{Q_{max}^{X} - Q^{X}}{Q_{max}^{X} - Q_{min}^{X}}\right)^{0.05} \quad (2)$$

where $V_{max}{}^{X}$ is the maximal uptake rate in mg of nutrient X per mg of cell C, X can represent N or Fe, Q is the nutrient cell quota and Q_{min} and Q_{max} its minimum and maximum values, and $V_{ref}{}^{X}$

https://doi.org/10.5194/gmd-2021-327
Preprint. Discussion started: 25 October 2021

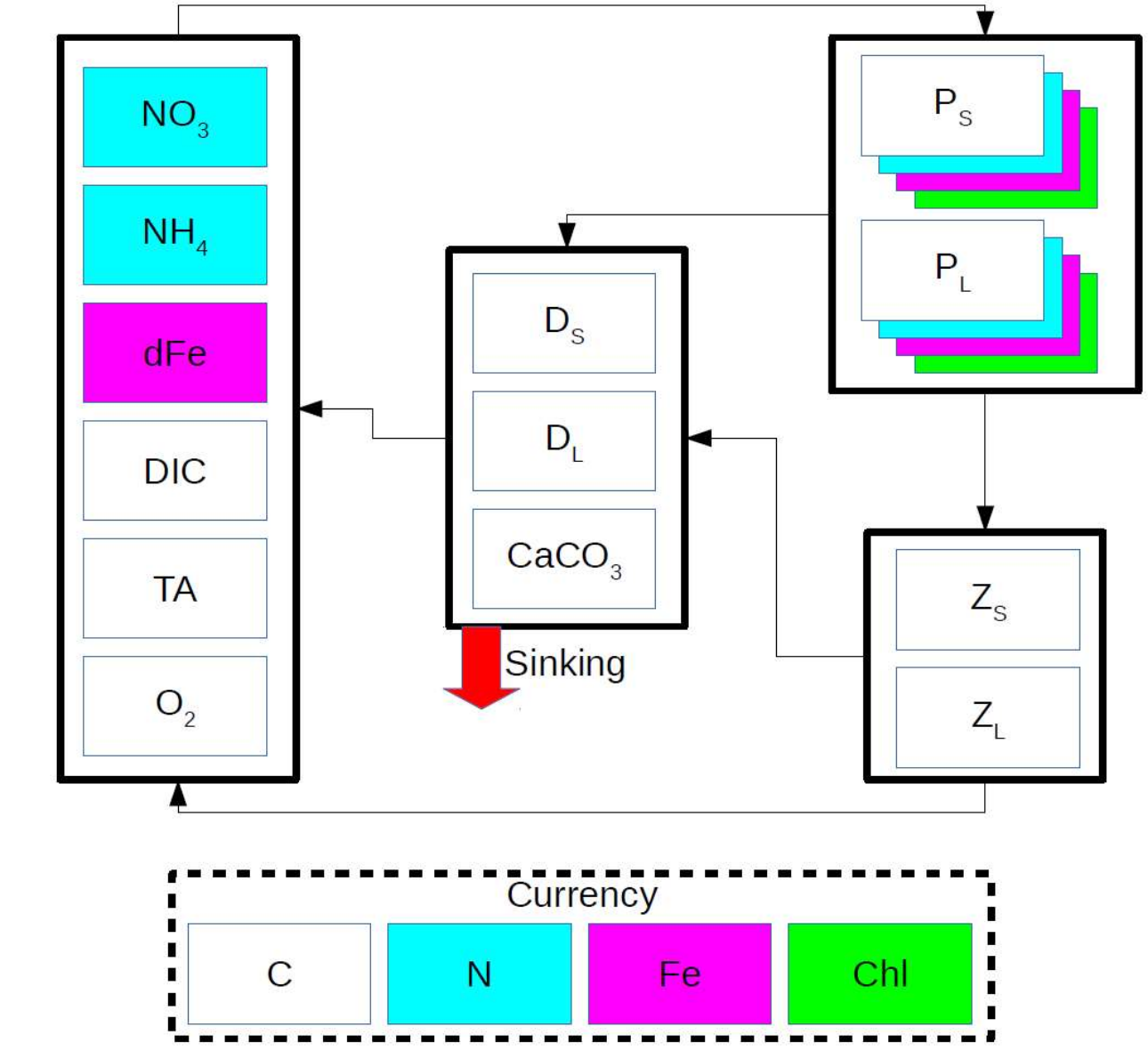

Figure 1 - Schematic of the CanOE biology model. Model currencies including chlorophyll (Chl) are indicated by coloured boxes except oxygen (O_2) and carbonate ($CaCO_3$). Arrows indicate flows of carbon (C), nitrogen (N) and iron (Fe) between compartments containing small (S) and large (L) phytoplankton (P), zooplankton (Z), and detritus (D) components; counterflows of oxygen are not shown.

https://doi.org/10.5194/gmd-2021-327
Preprint. Discussion started: 25 October 2021

Geoscientific Model Development Discussions

Table 1 – Ecosystem model parameters.

Symbol	Description	Unit	
T_{ref}	Reference temperature	K	298.15
E_{ap}	Activation energy for photosynthesis	kJ mol^{-1}	37.4
Q^{N}_{mins}	Small phytoplankton minimum N quota	g N g C^{-1}	0.04
Q^{N}_{maxs}	Small phytoplankton maximum N quota	g N g C^{-1}	0.172
Q^{N}_{minl}	Large phytoplankton minimum N quota	g N g C^{-1}	0.04
Q^{N}_{maxl}	Large phytoplankton maximum N quota	g N g C^{-1}	0.172
Q^{Fe}_{mins}	Small phytoplankton minimum Fe quota	µg Fe g C^{-1}	4.65
Q^{Fe}_{maxs}	Small phytoplankton maximum Fe quota	µg Fe g C^{-1}	93.
Q^{Fe}_{minl}	Large phytoplankton minimum Fe quota	µg Fe g C^{-1}	6.5
Q^{Fe}_{maxl}	Large phytoplankton maximum Fe quota	µg Fe g C^{-1}	70.
V^{N}_{ref}	Reference rate of N uptake	g N g C^{-1} d^{-1}	0.6
V^{Fe}_{ref}	Reference rate of Fe uptake	µg Fe g C^{-1} d^{-1}	79.
P^{C}_{ref}	Reference rate of photosynthesis	g C g C^{-1} d^{-1}	3
k_{XU}	Rate coefficient for exhudation	d^{-1}	1.7
k_{dgr}	Rate coefficient for chlorophyll degradation	d^{-1}	0.02
ζ	Respiratory cost of biosynthesis	g C g N^{-1}	2
α_{chl}	Initial slope of P-E curve	g C g CHL^{-1} h^{-1} (µmol m^{-2} s^{-1})$^{-1}$	1.08
Θ_{max}^{N}	Maximum chlorophyll-nitrogen ratio	g g^{-1}	0.18
K_{NiS}	Half-saturation for small phytoplankton nitrate uptake	$mmol^{-1}$ m^3	0.1
K_{NaS}	Half-saturation for small phytoplankton ammonium uptake	$mmol^{-1}$ m^3	0.05
K_{FeS}	Half-saturation for small phytoplankton iron uptake	$nmol^{-1}$ m^3	100
K_{NiL}	Half-saturation for large phytoplankton nitrate uptake	$mmol^{-1}$ m^3	1.0
K_{NaL}	Half-saturation for large phytoplankton ammonium uptake	$mmol^{-1}$ m^3	0.05
K_{FeL}	Half-saturation for large phytoplankton iron uptake	$nmol^{-1}$ m^3	200
m_{1S}	Small phytoplankton/zooplankton mortality rate (linear)	d^{-1}	0.05
m_{2S}	Small phytoplankton/zooplankton mortality coefficient	(mmol C m^{-3})$^{-1}$ d^{-1}	0.06
m_{1L}	Large phytoplankton/zooplankton mortality rate (linear)	d^{-1}	0.1

https://doi.org/10.5194/gmd-2021-327
Preprint. Discussion started: 25 October 2021

Geoscientific Model Development Discussions

m_{2L}	Large phytoplankton/zooplankton mortality coefficient	$(mmol\ C\ m^{-3})^{-1}\ d^{-1}$	0.06
X_{minp}	Minimum phytoplankton concentration for linear mortality	$mmol\ C\ m^{-3}$	0.01
a_L	Large zooplankton grazing parameter	$(mmol\ C\ m^{-3})^{-1}$	0.25
G_{L0}	Large zooplankton maximum grazing rate	d^{-1}	0.85
a_S	Small zooplankton grazing parameter	$(mmol\ C\ m^{-3})^{-1}$	0.25
G_{S0}	Small zooplankton maximum grazing rate	d^{-1}	1.7
λ	Assimilation efficiency	n.d.	0.8
r_{zs}	Microzooplankton specific respiration rate at T_{ref}	d^{-1}	0.3
r_{zl}	Mesozooplankton specific respiration rate at T_{ref}	d^{-1}	0.1
r_1	Small detritus remineralization rate at T_{ref}	d^{-1}	0.25
r_2	Large detritus remineralization rate at T_{ref}	d^{-1}	0.25
E_{ar}	Activation energy for detritus remineralization	$kJ\ mol^{-1}$	54.0
w_s	Small detritus sinking speed	$m\ d^{-1}$	2.
w_l	Large detritus sinking speed	$m\ d^{-1}$	30.
w_{Ca}	$CaCO_3$ sinking speed	$m\ d^{-1}$	20.
P_{Ca}	$CaCO_3$ production as fraction of mortality	$mol\ CaCO_3\ molC^{-1}$	0.05
k_{Ca}	$CaCO_3$ dissolution rate	d^{-1}	0.0074
S_{Fe1}	Dissolved iron scavenging loss rate ($Fe \leq L_{Fe}$)	d^{-1}	0.001
S_{Fe2}	Dissolved iron scavenging loss rate ($Fe > L_{Fe}$)	d^{-1}	2.5
L_{Fe}	Ligand concentration	$nmol\ Fe\ m^{-3}$	600.
P_{Fe}	POC-dependence parameter for Fe scavenging	$(mmolC\ m^{-3})^{-1}$	0.66
K_{NH4ox}	Nitrification rate in darkness	d^{-1}	0.05
K_E	Half-saturation for irradiance inhibition of nitrification	$W\ m^{-2}$	1.
k_{dnf}	Light and nutrient saturated rate of N_2 fixation at 30°C	$mmol\ m^{-3}\ d^{-1}$	0.0225
a	Initial slope for irradiance-dependence of N_2 fixation	$(W\ m^{-2})^{-1}$	0.02
K_{Fe}	Half-saturation for Fe dependence of N_2 fixation	$nmol\ m^{-3}$	100.
K_{NO3}	Half-saturation for DIN inhibition of N_2 fixation	$mmol\ m^{-3}$	0.1
O_{mxd}	O_2 concentration threshold for denitrification	$mmol\ m^{-3}$	6.
A_f	Anammox fraction of N loss to denitrification	n.d.	0.25

https://doi.org/10.5194/gmd-2021-327
Preprint. Discussion started: 25 October 2021


Geoscientific Model Development Discussions

158 is a (specified) basal rate at $T=T_{ref}$ and $Q=Q_{min}$. These maximum rates are then reduced according
159 to the ambient nutrient concentration, i.e.

160 $$V^N = V^N_{max}(L_{NH4} + (1 - L_{NH4})L_{NO3}) \quad (3a)$$

161 where $L_{\mathrm{NH4}} = \frac{N_a}{K_{\mathrm{NaX}}+N_a}$ and $L_{\mathrm{NO3}} = \frac{N_i}{K_{\mathrm{NiX}}+N_i}$, with N_i and N_a indicating nitrate and ammonium
162 respectively, and

163 $$V^{Fe} = V^{Fe}_{max}\left(\frac{\mathrm{Fe}}{K_{\mathrm{FeX}}+\mathrm{Fe}}\right) \quad (3b)$$

164 where X indicates large or small phytoplankton (Table 1). The maximal carbon-based growth
165 rate is given by

166 $$P^C_{max} = P^C_{ref}T_f \min\{\frac{Q^N - Q^N_{min}}{Q^N_{max} - Q^N_{min}} . \frac{Q^{Fe} - Q^{Fe}_{min}}{Q^{Fe}_{max} - Q^{Fe}_{min}}\} \quad (4)$$

167 where $P^C{}_{ref}$ is the rate at the reference temperature T_{ref} under nutrient-replete conditions
168 ($Q=Q_{max}$). The light-limited growth rate is then given by

169 $$P^C_{phot} = P^C_{max}\left(1 - e^{-\alpha_{chl}E\theta_C / P^C_{max}}\right) \quad (5)$$

170 where θ_C is the chlorophyll-to-carbon ratio. The rate of chlorophyll synthesis is

171 $$\rho_{\mathrm{chl}} = \theta^N_{max}\frac{P^C_{phot}}{E\alpha_{\mathrm{chl}}\theta} \quad (6)$$

172 These rates are then used to define a set of state equations for phytoplankton carbon (C_p),
173 nitrogen (N_p), iron (Fe_p), and chlorophyll (M).

174 $$\frac{\mathrm{dC}_p}{\mathrm{dt}} = (P^C_{phot} - \zeta V_N)C_p - (G + C_{\mathrm{XS}}) - m_1C_p - m_2C_p^2 - k_{\mathrm{XU}}C_{\mathrm{INTR}} \quad (7)$$

175 where ζ is the respiratory cost of biosynthesis, G is the grazing rate (equation 12), C_{XS} is the
176 excess (above the ratio in grazer biomass) carbon in grazing losses, m_1 and m_2 are coefficients
177 for linear and quadratic nonspecific mortality terms, C_{INTR} is the concentration of intracellular

https://doi.org/10.5194/gmd-2021-327
Preprint. Discussion started: 25 October 2021


Geoscientific Model Development Discussions

carbohydrate carbon in excess of biosynthetic requirements, and k_{XU} is a rate coefficient for its exudation to the environment. The nonspecific mortality terms are set to 0 below 0.01 mmol C m^{-3}, to prevent biomass from being driven to excessively low levels in the high latitudes in winter (Hayashida, 2018). The full equation for phytoplankton N, Fe and chlorophyll are

$$\frac{\mathrm{dN}_p}{\mathrm{dt}} = \frac{V^N}{Q_N} - (G + m_1 C_p + m_2 C_p^2) R_{\mathrm{NC}} - N_{\mathrm{XS}} \quad (8)$$

$$\frac{\mathrm{dFe}_p}{\mathrm{dt}} = \frac{V^{\mathrm{Fe}}}{Q_{\mathrm{Fe}}} - (G + m_1 C_P + m_2 C_p^2) R_{\mathrm{FeC}} - \mathrm{Fe}_{\mathrm{XS}} \quad (9)$$

$$\frac{\mathrm{dM}}{\mathrm{dt}} = \frac{\rho_{\mathrm{chl}} V^N}{\theta_C} M - (G + m_1 C_p + m_2 C_p^2) \theta_C - k_{\mathrm{dgr}} M \quad (10)$$

where k_{dgr} is a rate coefficient for nonspecific losses of chlorophyll e.g., by photooxidation, in addition to losses to grazing and other processes that also affect C_p, N_p, and Fe_p. N_{XS} and Fe_{XS} are remineralization of "excess" (relative to grazer or detritus ratios) N or Fe and are defined below (equation 16).

2.2 Grazing and Food Web Interactions

Grazing rate depends on the phytoplankton carbon concentration, which most closely represents the food concentration available to the grazer (Elser and Urabe 1999; Loladze et al. 2000). Zooplankton biomass is also in carbon units. State equations for small and large zooplankton are

$$\frac{\mathrm{dZ}_s}{\mathrm{dt}} = \lambda G_s - (R + G_Z + m_{1s} Z_s + m_{2s} Z_s^2) \quad (11a)$$

$$\frac{dZ_L}{\mathrm{dt}} = \lambda G_L - (R + m_{1L} Z_L + m_{2L} Z_L^2) \quad (11b)$$

where

https://doi.org/10.5194/gmd-2021-327
Preprint. Discussion started: 25 October 2021


Geoscientific Model Development Discussions

$$G_s = G_{so}(1 - e^{-a_s C_{ps}})Z_s \quad (12a)$$

$$G_L = G_{L0}(1 - e^{-a_l (C_{pl} + Z_s)})Z_L \quad (12b)$$

for small and large zooplankton respectively, G_Z is grazing of small zooplankton by large zooplankton, R is respiration, and m_1 and m_2 are nongrazing mortality rates. Large zooplankton grazing is divided into grazing on large phytoplankton and small zooplankton in proportion to the relative abundance of each

$$G_P = G_L \frac{P_l}{P_l + Z_s} \quad (13a)$$

$$G_Z = G_{lL} \frac{Z_s}{P_l + Z_s} \quad (13b)$$

Zooplankton biomass loss to respiration is given by

$$R = max\{r_z T_f Z - C_{XS}. 0\} \quad (14)$$

and uses the same activation energy as photosynthesis. Respiration (R) is assumed to consume only carbon and not result in catabolism of existing biomass when "excess" carbon is available in the prey. In addition, conservation of mass must be maintained by recycling to the dissolved pool grazer consumption of elements in excess of biosynthetic requirements when grazer and prey elemental ratios differ. In the case where the nutrient quota (relative to carbon) exceeds the grazer fixed ratio, the excess nutrient is remineralized to the dissolved inorganic pool. In the case where the nutrient quota is less than the grazer ratio, the grazer intake is reduced to what can be supported by the least abundant nutrient (relative to the grazer biomass ratio) and excess carbon is remineralized. For the case of two nutrients (in this case N and Fe) it is necessary to define

$$G' = G\min\left\{\frac{N_P}{C_P} R_{CN}, \frac{Fe_P}{C_P} R_{CFe}, 1\right\} \quad (15)$$

https://doi.org/10.5194/gmd-2021-327
Preprint. Discussion started: 25 October 2021

Geoscientific Model Development Discussions

where G is equal to G_S (equation 12a) for small zooplankton and G_P (equation 13a) for large zooplankton, and R_{XY} indicates the fixed ratio of element X to element Y in grazer biomass. The 'excess' carbon available for respiration is

$$C_{\mathrm{XS}} = G'\left\{\frac{C_P}{N_P}R_{\mathrm{NC}} - 1, \frac{C_P}{\mathrm{Fe}_P}R_{\mathrm{FeC}} - 1, 0\right\} \quad (16a)$$

and the excess nutrients remineralized to their inorganic pools are

$$N_{\mathrm{XS}} = G'\max\left\{\frac{N_P}{C_P} - R_{\mathrm{NC}}.0\right\}\varepsilon + G'\max\left\{R_{\mathrm{NC}}\left(\frac{N_P}{\mathrm{Fe}_P}R_{\mathrm{FeN}} - 1\right).0\right\}(1-\varepsilon) \quad (16b)$$

$$\mathrm{Fe}_{\mathrm{XS}} = G'\max\left\{\frac{\mathrm{Fe}_P}{C_P} - R_{\mathrm{FeC}}.0\right\}\varepsilon + G'\max\left\{R_{\mathrm{FeC}}(\frac{\mathrm{Fe}_P}{N_P}R_{\mathrm{NFe}} - 1).0\right\}(1-\varepsilon) \quad (16c)$$

where

$$\varepsilon = \frac{\max\{C_{\mathrm{xs}}, 0\}}{C_{\mathrm{xs}} + \Delta}$$

is a switch to prevent double-counting in cases where one of the terms is redundant (the excess relative to the least abundant element is included in the other term), but would otherwise be nonzero (Δ is a constant equal to 10^{-15}, to prevent divide-by-zero). For three elements, there are 3! = 6 possible cases: for N greater or less than $C_P R_{NC}$, Fe may be either in excess relative to both C and N, deficient relative to both, or in excess relative to one but not the other (Table 2).

Table 2 - Cases where the 'excess' terms are nonzero. These terms are always greater than or equal to zero, and always zero when the phytoplankton elemental ratio is equal to the grazer biomass ratio. A plus (+) sign indicates that a specific term is positive. N_1 and N_2, Fe_1 and Fe_2 indicate the first and second terms in equations 16b and 16c. R_{NC} is the grazer N/C (Redfield) ratio.

	Fe in excess relative to both C and N					Fe in excess relative to C or N but not both					Fe deficient relative to both C and N				
	C	N_1	N_2	Fe_1	Fe_2	C	N_1	N_2	Fe_1	Fe_2	C	N_1	N_2	Fe_1	Fe_2
$N/C>R_{NC}$		+		+			+		+		+		+		
$N/C<R_{NC}$	+				+	+				+	+		+		

https://doi.org/10.5194/gmd-2021-327
Preprint. Discussion started: 25 October 2021

Geoscientific Model Development Discussions

2.3 Organic and Inorganic Pools

There are two pools of detritus with different sinking rates but the same fixed elemental ratios. Detrital C/N/Fe ratios are the same as zooplankton, so zooplankton mortality or grazing of small zooplankton by large zooplankton produce no 'excess'. Phytoplankton mortality, and defecation by zooplankton grazing on phytoplankton, produces excess nutrient or excess C that needs to be recycled into the inorganic pool in a similar fashion as outlined above for the assimilated fraction of grazing on phytoplankton.

The conservation equations for detrital C are

$$\frac{\mathrm{dD}_s}{\mathrm{dt}} = m_1(C_{\mathrm{ps}} + Z_s) + m_2(C_{ps}^2 + Z_S^2) - r_1 D_s T_g - w_s \frac{\mathrm{dD}_s}{\mathrm{dz}} \quad (17a)$$

$$\frac{\mathrm{dD}_l}{\mathrm{dt}} = m_1(C_{\mathrm{pl}} + Z_L) + m_2(C_{pl}^2 + Z_L^2) - r_2 D_l T_g - w_l \frac{\mathrm{dD}_l}{\mathrm{dz}} \quad (17b)$$

where T_g is an Arrhenius function for temperature dependence of remineralization and w is the sinking speed. The conservation equations for inorganic C, N, and Fe are

$$\frac{\mathrm{dC}_i}{\mathrm{dt}} = (\zeta V^N - P_{\mathrm{phot}}^C)C_p + R + C_{\mathrm{XS}} + (r_1 D_s + r_2 D_l)T_g \quad (18a)$$

$$\frac{\mathrm{dN}_i}{\mathrm{dt}} = -\frac{V^N}{Q^N} N_p \left(\frac{L_{\mathrm{NO3}}}{L_{\mathrm{NO3}} + L_{\mathrm{NH4}}}\right) + N_{\mathrm{ox}} - N_{\mathrm{dentr}}(1 - A_f) \quad (18b)$$

$$\frac{\mathrm{dN}_a}{\mathrm{dt}} = -\frac{V^N}{Q^N} N_p \left(\frac{L_{\mathrm{NH4}}}{L_{\mathrm{NO3}} + L_{\mathrm{NH4}}}\right) + \frac{R}{R_{\mathrm{CN}}} + N_{\mathrm{XS}} + (r_1 D_s + r_2 D_l) R_{\mathrm{NC}} T_g - N_{\mathrm{ox}} + N_{\mathrm{dnf}} - N_{\mathrm{dentr}} A_f \quad (18c)$$

$$\frac{\mathrm{dFe}}{\mathrm{dt}} = \frac{V^{\mathrm{Fe}}}{Q^{\mathrm{Fe}}} \mathrm{Fe}_p + \frac{R}{R_{\mathrm{CFe}}} + \mathrm{Fe}_{\mathrm{XS}} + (r_1 D_s + r_2 D_l) R_{\mathrm{FeC}} T_g \quad (18d)$$

where N_{ox} is microbial oxidation of ammonium to nitrate (nitrification), N_{dnf} and N_{dentr} are sources and sinks associated with dinitrogen fixation and denitrification, and A_f is the ammonium fraction of denitrification losses, associated with anaerobic ammonium oxidation ("anammox").

https://doi.org/10.5194/gmd-2021-327
Preprint. Discussion started: 25 October 2021

Geoscientific Model Development Discussions

The oxygen equation is essentially the inverse of equation 18a, with additional terms for oxidation and reduction of N, i.e.,

$$\frac{\mathrm{dO_2}}{\mathrm{dt}} = -\frac{\mathrm{dC}_i}{\mathrm{dt}} + 2\frac{V^N}{Q^N}N_p\left(\frac{L_{\mathrm{NO3}}}{L_{\mathrm{NO3}}+L_{\mathrm{NH4}}}\right) - 2N_{\mathrm{ox}} \quad (19)$$

Nitrification is given by

$$N_{\mathrm{ox}} = k_{\mathrm{NH4ox}}N_a\frac{K_E}{K_E+E(z)} \quad (20)$$

where $E(z)$ is the layer mean irradiance at depth z. Dinitrogen fixation is parameterized as an external input of ammonium dependent on light, temperature and Fe availability, and inhibited by high ambient concentrations of inorganic N,

$$N_{\mathrm{dnf}} = k_{\mathrm{dnf}}T_{\mathrm{dnf}}(1-e^{-\mathrm{aE}})\left(\frac{\mathrm{Fe}}{K_{\mathrm{Fe}}+\mathrm{Fe}}\right)\left(\frac{K_{\mathrm{NO3}}}{K_{\mathrm{NO3}}+N_i+N_a}\right) \quad (21)$$

where T_{dnf}=max(0, 1.962(T_f - 0.773)), i.e., a linear multiple of equation (1) that is 0 at T<20°C and unity at T=30°C.

Denitrification is parameterized as a fraction of total remineralization that increases as a linear function of oxygen concentration for concentrations less than a threshold concentration O_{mxd}

$$N_{\mathrm{frxn}} = 1 - \frac{\min(O_2, O_{\mathrm{mxd}})}{O_{\mathrm{mxd}}} \quad (22)$$

Remineralization is then divided among oxygen (1-N_{frxn}), nitrate (0.875N_{frxn}), and ammonium (0.125N_{frxn}) assuming an average anammox contribution of 25% (Babbin et al., 2014). We use this average ratio of anammox to classical denitrification to partition fixed N losses between NO_3^- and NH_4^+; the DIC sink and organic matter source associated with anammox are small and are neglected here.

https://doi.org/10.5194/gmd-2021-327
Preprint. Discussion started: 25 October 2021

Geoscientific Model Development Discussions

279 **2.4 Calcification, Calcite Dissolution, and Alkalinity**

280

281 Calcification is represented by a detrital calcium carbonate ($CaCO_3$) state variable, but no
282 explicit calcifier groups. Detrital $CaCO_3$ sinks in the same fashion as detrital particulate organic
283 carbon (POC), with a sinking rate independent of those for large and small organic detritus.
284 Calcite production is represented as a fixed fraction of detritus production from small
285 phytoplankton and small zooplankton mortality:

286 $$\frac{dCa}{\mathrm{dt}} = m_1\left(C_{\mathrm{ps}} + Z_s\right)P_{Ca} + m_2\left(C_{ps}^2 + Z_S^2\right)P_{Ca} - k_{Ca}Ca - w_{Ca}\frac{dCa}{\mathrm{dz}} \quad (23)$$

287 Calcite dissolution occurs throughout the water column as a first order process (i.e., no
288 dependence on temperature or saturation state). Approximately 80% of calcite produced is
289 exported from the euphotic zone. Burial in the sediments is represented as a simple 'on/off'
290 switch dependent on the calcite saturation state (zero when $\Omega_C<1$ and 1 when $\Omega_C\geq1$). Calcite
291 burial is balanced by an equivalent source of DIC and alkalinity at the ocean surface as a crude
292 parameterization of fluvial sources.

293

294 For each mole of calcite production two moles of alkalinity equivalent are lost from the
295 dissolved phase; the reverse occurs during calcite dissolution. There are additional sources and
296 sinks for alkalinity associated with phytoplankton nutrient uptake, organic matter
297 remineralization, nitrification, denitrification and dinitrogen fixation (Wolf-Gladrow et al., 2007,
298 see Supplementary Table S2). The anammox reaction does not in itself contribute to alkalinity
299 (Jetten at al., 2001), but there is a sink associated with ammonium oxidation to nitrite (the model
300 does not distinguish between nitrite and nitrate). Autotrophic production of organic matter by
301 anammox bacteria is a net source of alkalinity (Strous et al., 1998) but this source is extremely

https://doi.org/10.5194/gmd-2021-327
Preprint. Discussion started: 25 October 2021


Geoscientific Model Development Discussions

small (~0.03 mol/molN) and is neglected here. Globally, the sources and sinks of alkalinity from the N cycle offset each other such that there is no net gain or loss as long as the global fixed N pool is conserved (see below Sect. 2.5). If dinitrogen fixation and denitrification are allowed to vary freely, there will generally be a net gain or loss of fixed N and, therefore, of alkalinity.

2.5 External Nutrient Sources and Sinks

External sources and sinks consist of river inputs, aeolian deposition, biological N_2 fixation, denitrification, mobilization of Fe from reducing sediments, loss of Fe to scavenging, and burial of calcium carbonate in the sediments. Aeolian deposition of Fe is calculated from a climatology of mineral dust deposition generated from offline (atmosphere-only) simulations with CanAM4 (von Salzen et al., 2013), with an Fe mass fraction of 5% and a fractional solubility of 1.4% in the surface layer. Subsurface dissolution is parameterized based on PISCES (Aumont et al., 2015); the total dissolution is 6.35%, with 22% of soluble Fe input into the first vertical layer (see Supplementary material). Iron from reducing sediments is also based on PISCES, with a constant areal flux of 1000 nmol m^{-2} d^{-1} in the first model level, declining exponentially with increasing seafloor depth (i.e., assuming that the sediments become progressively more oxygenated) with an e-folding length scale of about 200 m. Scavenging of dissolved iron is first-order with a high rate (2.5 d^{-1}) for concentrations in excess of 0.6 nM (Johnson et al., 1997). For concentrations below this threshold, the rate is much lower (0.001 d^{-1}) and is weighted by the concentration of organic detritus (Christian et al., 2002b), i.e.,

$$\frac{dFe}{dt} = -FeS_{Fe1}min\{(D_S + D_L)P_{Fe}, 1\} \quad (24)$$

https://doi.org/10.5194/gmd-2021-327
Preprint. Discussion started: 25 October 2021


Geoscientific Model Development Discussions

where Fe is the dissolved iron concentration, D_S and D_L are the small and large detritus concentrations, S_{Fe1} is the first-order scavenging rate in surface waters with abundant particulates, and P_{Fe} is an empirical parameter to determine the dependence on particle concentration (Table 1). The basis for this parameterization is that the rate of scavenging must depend not only on the concentration of iron but on the concentration of particles available for it to precipitate onto, and assumes that POC is strongly positively correlated with total particulate matter. Scavenging is treated as irreversible, i.e., scavenged Fe is not tracked and does not reenter the dissolved phase.

Unlike in CMOC, N_2 fixation and denitrification vary independently in CanOE, so the global total N pool can change. Conservation is imposed by adjusting the global total N pool according to the difference between the gain from N_2 fixation and the loss to denitrification. A slight adjustment is applied to the nitrate concentration at every grid point, while preserving the overall spatial structure of the nitrate field. Adjustments are multiplicative rather than additive to avoid producing negative concentrations. This adjustment does not maintain (to machine precision) a constant global N inventory but is intended to minimize long term drift, keeping it much smaller than the free surface error (see below). This adjustment is applied every 10 days and has a magnitude of approximately $7x10^{-8}$ of the total N.

One mole of alkalinity is removed per mole of N added or removed, since there are alkalinity sources of 1 mol/molN associated with both N_2 fixation (creation of new NH_4^+) and denitrification (removal of NO_3^-), offset by a 2 mol/molN sink associated with nitrification. As noted above, $CaCO_3$ can dissolve or be buried in the sediments depending on the calcite saturation. DIC and alkalinity lost to burial are reintroduced at the ocean surface, at the same grid

https://doi.org/10.5194/gmd-2021-327
Preprint. Discussion started: 25 October 2021


Geoscientific Model Development Discussions

point as burial occurs, providing a crude parameterization of river inputs so that global conservation is maintained (fresh water runoff contains no DIC or alkalinity). However, the OPA free surface formulation is inherently imperfect with regard to tracer conservation. Drift in total ocean alkalinity and nitrogen over time is on the order of 0.01% and 0.03% per thousand years, respectively (losses due to the free surface are generally larger for tracers with less homogeneous distributions).

2.6 Ancillary data

For first-order model validation we have relied largely on global gridded data products rather than individual profile data. Global gridded data from World Ocean Atlas 2013 (WOA2013) (Locarnini et al., 2013; Zweng et al., 2013; Garcia et al., 2014a; 2014b) were used for temperature, salinity, and oxygen and nitrate concentration. DIC and alkalinity were taken from the GLODAP gridded data product (Lauvset et al., 2016). Offline carbon chemistry calculations were done following the Best Practices Guide (Dickson et al., 2007) and the OMIP-BGC protocols (Orr et al., 2017), which are identical to those used in the models except that constant reference concentrations were used for phosphate (1 µM) and silicate (10 µM).

There is no global gridded data product for Fe, but we have made use of the GEOTRACES Intermediate Data Product 2017 (Schlitzer et al., 2018), and the data compilations from MBARI (Johnson et al., 1997; 2003) and PICES Working Group 22 (Takeda et al., 2013). The latter two are concentrated in the Pacific, while GEOTRACES is more global. The combined data sets provide more than 10000 bottle samples from more than 1000 different locations (Supplementary

https://doi.org/10.5194/gmd-2021-327
Preprint. Discussion started: 25 October 2021


Geoscientific Model Development Discussions

Figure S4a) (excluding some surface transect data that involve frequent sampling of closely spaced locations along the ship track). More detail about model comparison to these data compilations and the list of original references are given in the Supplementary information.

Satellite ocean colour estimates of surface chlorophyll were taken from the combined SeaWiFS/MODIS climatology described by Tesdal et al. (2016). Climatological satellite POC was downloaded from the NASA ocean colour web site and is based on the algorithm of Stramski et al. (2008) using MODIS-Aqua data. This climatology differs slightly from the chlorophyll one in terms of years included and sensors utilized, but as only climatological concentrations are considered and each climatology covers ~15 years, these differences will have negligible effect on the results presented.

CMIP6 model data were regridded to a common grid (2x2°, 33 levels following the GLODAP levels) to facilitate ensemble averaging. The years 1986-2005 of the Historical experiment were averaged into climatologies or annual means, for meaningful comparison with observation-based data products. A single realization was used in each case; as 20 year averages are used, internal variability is assumed to have little effect (e.g., Arguez and Vose, 2011). Sampling among CMIP6 models was somewhat opportunistic and the exact suite of models varies among the analyses presented. When we conducted a search for a particular data field, we included in the search parameters all models that published that field, and repeated the search at least once for models that were unavailable the first time the search was executed. In some cases, model ensemble means excluded all but one model from a particular 'family' (e.g., there are three different MPI-ESM models for which ocean biogeochemistry fields were published), as the

https://doi.org/10.5194/gmd-2021-327
Preprint. Discussion started: 25 October 2021


Geoscientific Model Development Discussions

393 solutions were found to be similar and would bias the ensemble mean towards their particular
394 climate. More detail is given in Supplementary Table S3.
395
396 **3. Results**
397
398 **3.1 Distribution of oxygen**
399
400 The spatial distribution of oxygen concentration ([O_2]) at selected intermediate depths (400, 900,
401 and 1400 m) for CanESM5, CanESM5-CanOE, a model ensemble mean (MEM) of CMIP6
402 models (excluding CanESM5 and CanESM5-CanOE), and gridded data from WOA2013 is
403 shown in Figure 2. The major features are consistent across the models. All three cases show
404 elevated oxygen concentrations relative to observations, particularly in the North Pacific, the
405 North Atlantic and the Southern Ocean. In the Indian Ocean, both CanESM models show high
406 oxygen concentrations in the Arabian Sea and deeper layers of the Bay of Bengal relative to
407 observations and other CMIP6 models; these biases are somewhat smaller in CanESM5-CanOE
408 than in CanESM5 (Figure 2).
409
410 Biases in the eastern boundary current regions are depth and model specific. CanESM5 shows
411 particularly strong oxygen depletion at 1400 m in the eastern tropical Pacific. In the southeastern
412 Atlantic, models tend to be biased low at the shallower depths, and show somewhat more
413 variation at greater depths (Figure 2). Overall, [O_2] biases tend to be positive over large areas of
414 ocean with the exception of some eastern boundary current regions, implying that models
415 exaggerate the extent to which remineralization is concentrated in these regions. An alternate

https://doi.org/10.5194/gmd-2021-327
Preprint. Discussion started: 25 October 2021

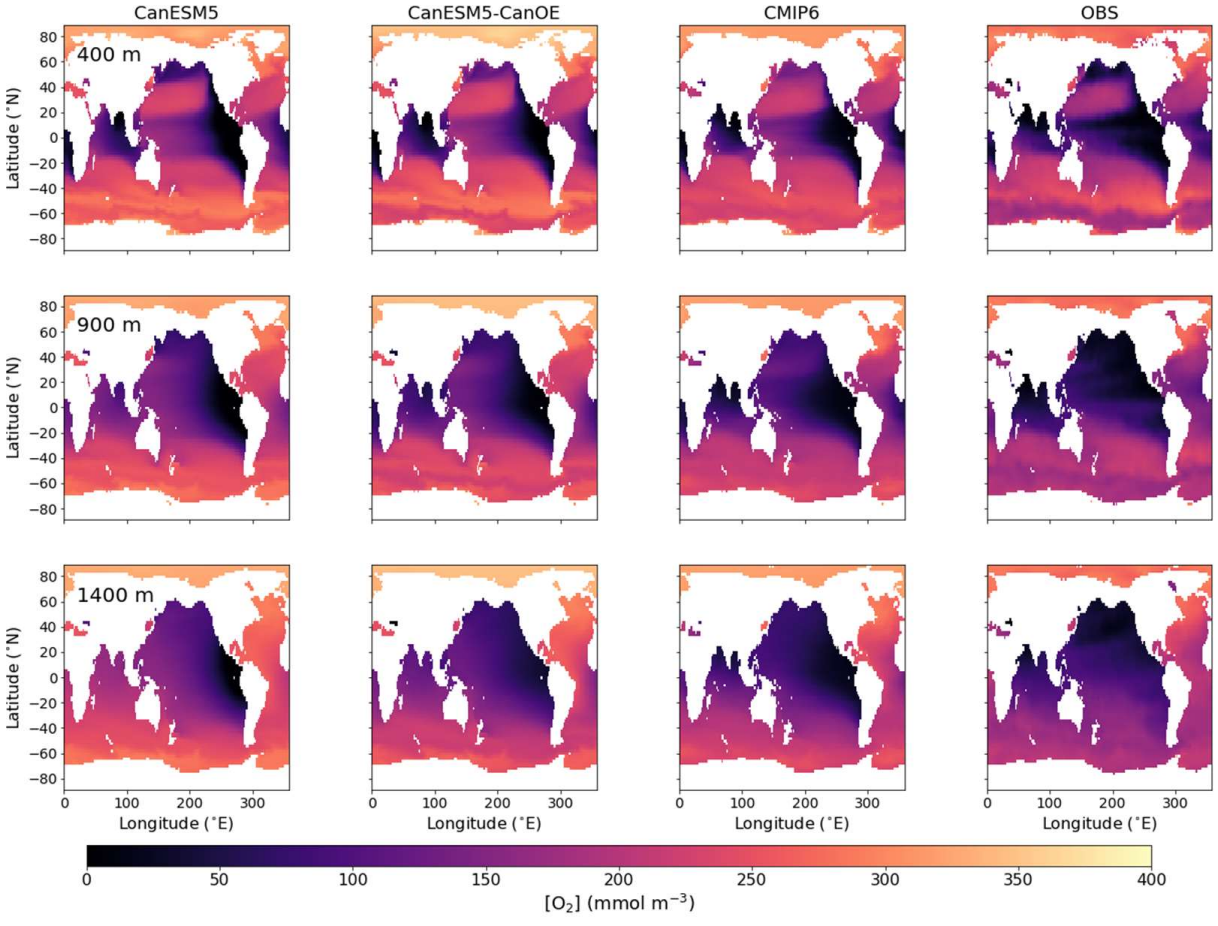

Figure 2 - Global distribution of oxygen (O_2) concentration in mmol m^{-3} at 400, 900, and 1400 m (rows) for CanESM5-CanOE, CanESM5, the mean for other (non-CanESM) CMIP6 models, and World Ocean Atlas 2013 (WOA2013) observations (columns). Difference from the observation-based fields are shown in Supplementary Figure S3.

https://doi.org/10.5194/gmd-2021-327
Preprint. Discussion started: 25 October 2021


Geoscientific Model Development Discussions

417 version of Figure 2 that shows model errors relative to the observational data product is given in
418 Supplementary Figure S3.
419
420 The zonal mean oxygen concentration, saturation concentration, and apparent oxygen utilization
421 (AOU) are shown in Figure 3 for the same four cases. Again, the models generally show a
422 positive bias in [O_2], particularly in high-latitude deep waters. The major ocean circulation
423 features are reproduced fairly well in all cases (e.g., weaker ventilation of low-latitude
424 subsurface waters, greater vertical extent of well-ventilated surface waters in the subtropics). The
425 saturation concentration (a function of temperature and salinity) generally shows relatively little
426 bias, implying that the bias in [O_2] arises mainly from remineralization and/or ventilation. AOU
427 is lower than observed over much of the subsurface ocean. Regional biases are quite consistent
428 across models, but are slightly greater in CanESM5 than in CanESM5-CanOE or the ensemble
429 mean, except in the Arctic Ocean. Again, Supplementary Figure S3 includes a version of this
430 plot that shows the model differences from the observations.
431
432 The skill of each model with respect to the distribution of O_2 at different depths is represented by
433 Taylor diagrams (Taylor, 2001) in Figure 4, in which all of the CMIP6 models that were shown
434 as an ensemble mean in Figures 2 and 3 are shown individually. The blue dots represent
435 CanESM5, red CanESM5-CanOE, and grey the ensemble mean of all CMIP6 models except
436 CanESM5 and CanESM5-CanOE; the smaller grey dots represent the individual models.
437 CanESM5-CanOE shows slightly higher pattern correlation than CanESM5 at all depths. Both
438 models compare favourably with the full suite of CMIP6 models, with $r>0.85$ for CanESM5 and
439 $r>0.9$ for CanESM5-CanOE at all depths examined, and a normalized standard deviation within

https://doi.org/10.5194/gmd-2021-327
Preprint. Discussion started: 25 October 2021

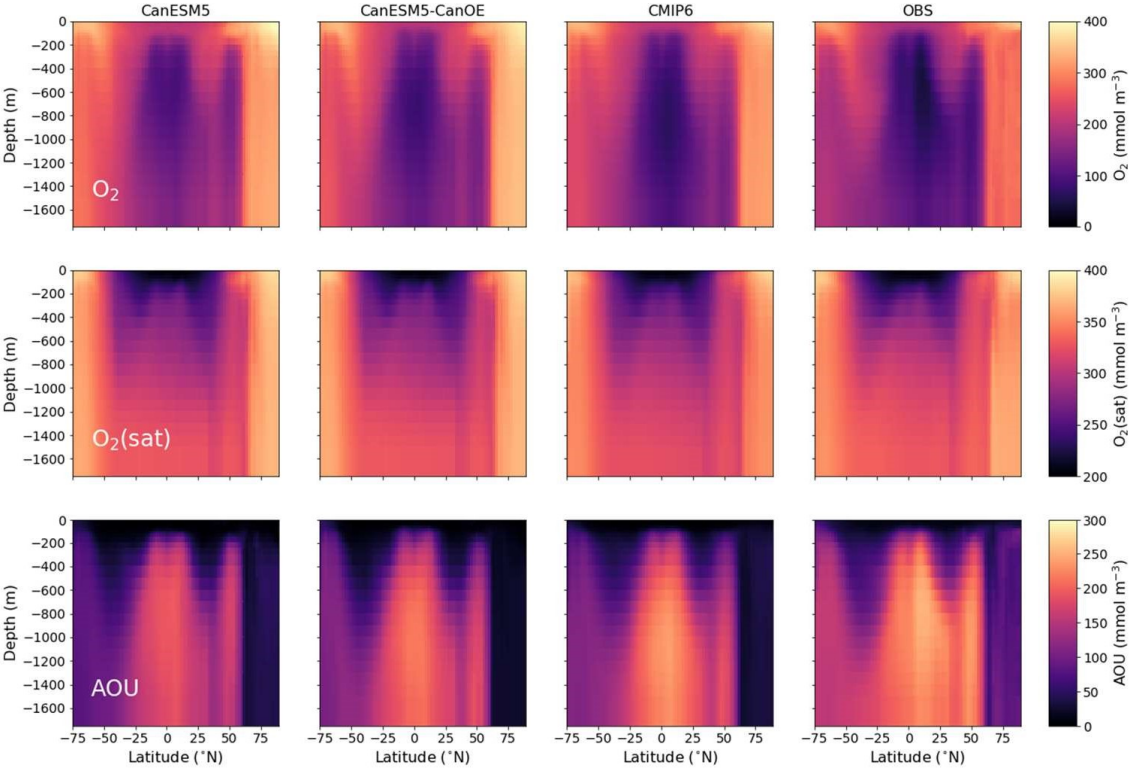

Figure 3 - Latitude-depth distribution (surface to 1750 m) of zonal mean oxygen concentration (O_2), oxygen concentration at saturation (O_2(sat)), and apparent oxygen utilization (AOU) in mmol m^{-3} for CanESM5-CanOE, CanESM5, the mean for other CMIP6 models, and observations (WOA2013). Note different colour scales for different rows. Difference from the observation-based fields are shown in Supplementary Figure S3.

https://doi.org/10.5194/gmd-2021-327
Preprint. Discussion started: 25 October 2021

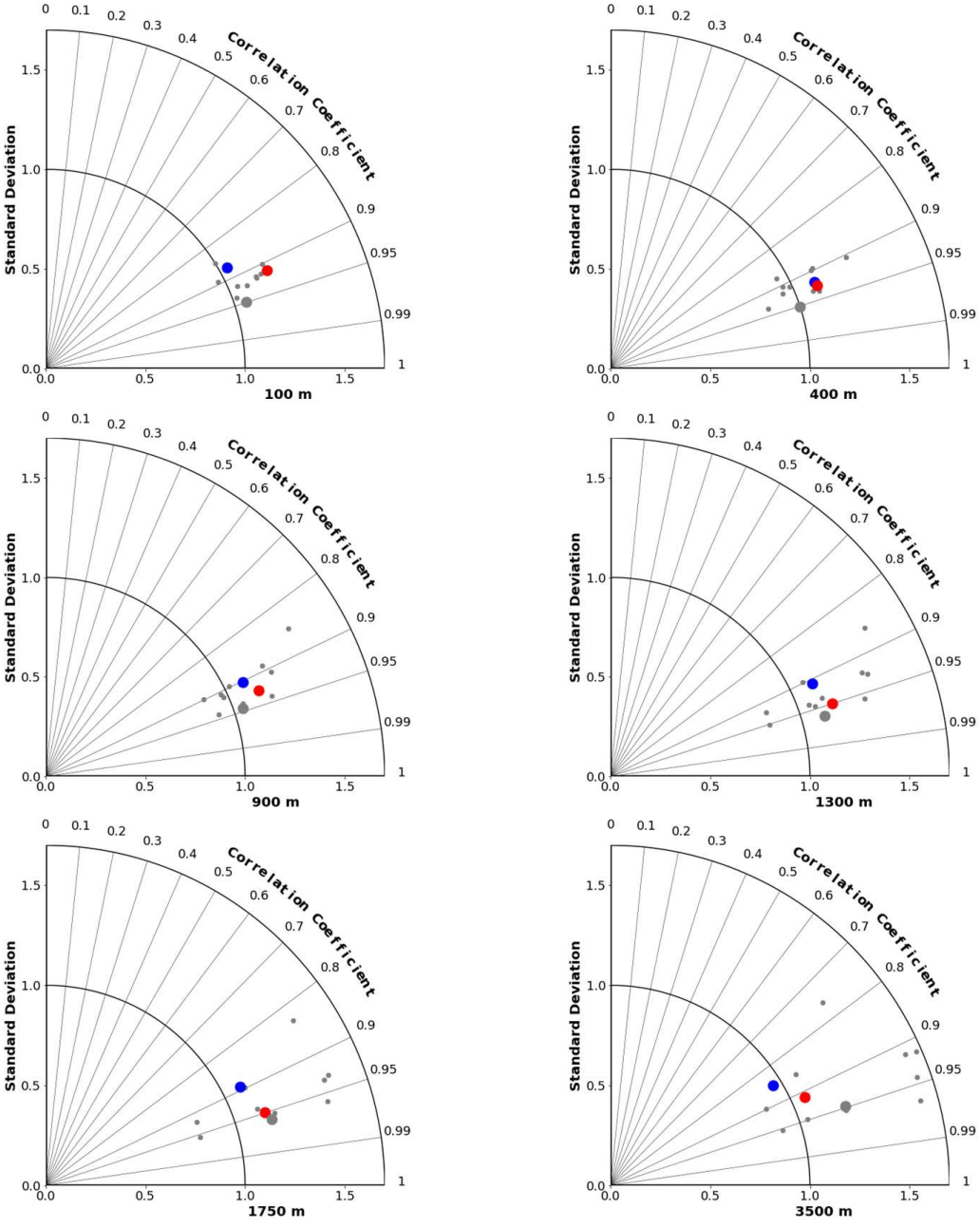

Figure 4 - Taylor diagrams (Taylor, 2001) comparing modelled and observed distributions of oxygen at specific depths from 100 to 3500 m. Angle from the vertical indicates spatial pattern correlation. Distance from the origin indicates ratio of standard deviation in modelled vs. observed (WOA2013) fields. Red dots represent CanESM5-CanOE, blue dots CanESM5, small grey dots other CMIP6 models, and large grey dots the model ensemble mean for all CMIP6 models except CanESM5 and CanESM5-CanOE.

https://doi.org/10.5194/gmd-2021-327
Preprint. Discussion started: 25 October 2021


Geoscientific Model Development Discussions

±25% of unity.

The total volume of ocean with [O_2] less than 6 mmol m^{-3} (the threshold for denitrification (Devol, 2008)) and 60 mmol m^{-3} (a commonly used index of hypoxia) is shown in Figure 5. The total volume is highly variable among models (note, however, that there are several clusters of related models with quite similar totals). CanESM5 and CanESM5-CanOE have among the lowest total volumes (i.e., the interior ocean is relatively well ventilated) and are among the nearest to the observed total. For [O_2] <60 mmol m^{-3} the bias is, nonetheless, quite large (i.e., the observed volume is underestimated by almost 50% in both models). The volume of water with [O_2] below the denitrification threshold is overestimated in both CanESM5 and CanESM5-CanOE; CanESM5-CanOE has a much smaller total that is closer to the observed value. The bias in the spatial pattern of hypoxia (not shown) is generally similar to the bias in dissolved oxygen distribution (Figure 2). The low-oxygen regions are generally more concentrated in the eastern tropical Pacific in the models than in observations, and the low-oxygen region in the northwest Pacific is not well reproduced in CanESM models.

3.2 Distribution of DIC, alkalinity, and $CaCO_3$ saturation

The spatial distribution of aragonite saturation state (Ω_A) at selected depths is shown in Figure 6 (the first two depths are the same as in Figure 2, but the third is much deeper). In this case the observations are a combination of GLODAP (Lauvset et al., 2016) for DIC and alkalinity, and WOA2013 for temperature and salinity. CanESM5 and CanESM5-CanOE generally compare well with other models and observations. The low saturation bias in the eastern tropical Pacific is

https://doi.org/10.5194/gmd-2021-327
Preprint. Discussion started: 25 October 2021

Geoscientific Model Development Discussions

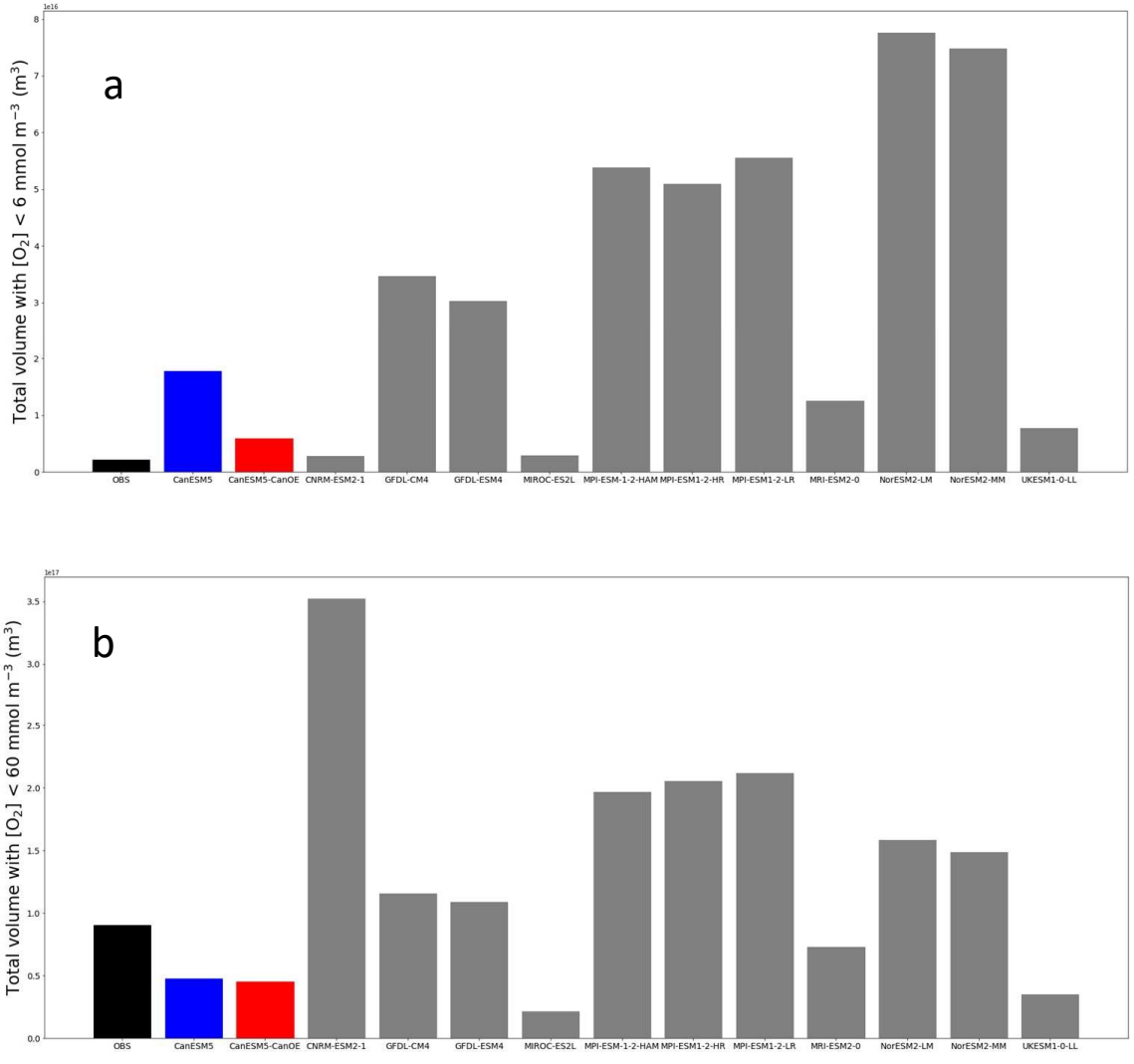

Figure 5 - Total volume of ocean with oxygen (O_2) concentration less than (a) 6 mmol m^{-3} (mean for last 30 years of the historical experiment) and (b) 60 mmol m^{-3}. Observation are from WOA2013.

https://doi.org/10.5194/gmd-2021-327
Preprint. Discussion started: 25 October 2021

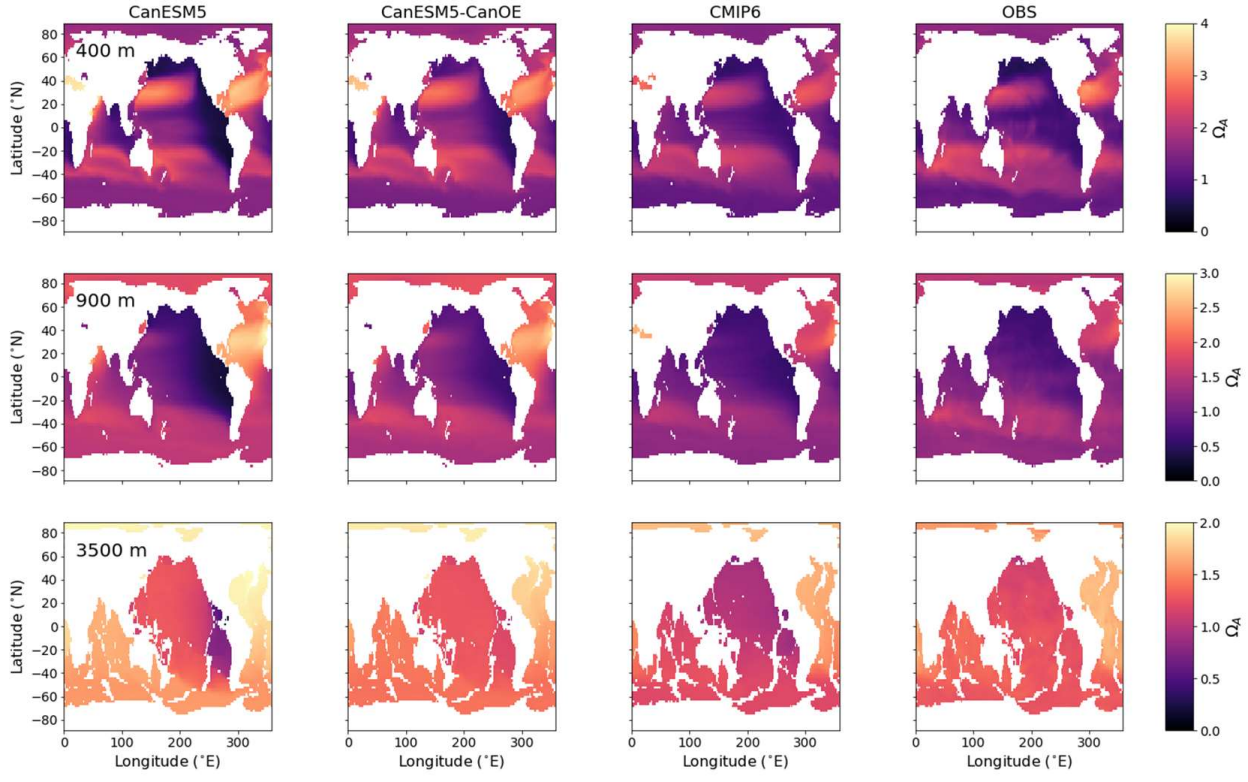

Figure 6 - Global distribution of aragonite saturation (Ω_A) at 400, 900, and 3500 m for CanESM5-CanOE, CanESM5, the mean for other CMIP6 models, and observations (GLODAP + WOA2013). Note different colour scales for different depths. Difference from the observation-based fields are shown in Supplementary Figure S3.

https://doi.org/10.5194/gmd-2021-327
Preprint. Discussion started: 25 October 2021


Geoscientific Model Development Discussions

substantially reduced in CanESM5-CanOE compared to CanESM5. On the other hand CanESM5 generally does better than CanESM5-CanOE, or the ensemble mean, at reproducing the low saturation states in the northwestern Pacific and the Bering Sea. Both models show a high saturation state bias in the North Atlantic and the well-ventilated regions of the north Pacific subtropical gyre. These biases are reduced slightly in CanESM5-CanOE, probably due to the smaller average remineralization length scale for organic detritus.

Zonal mean distributions of aragonite saturation state (Ω_A), calcite saturation state (Ω_C), and carbonate ion concentration ($[CO_3^{--}]$) are shown in Figure 7 (Supplementary Figure S3 includes versions of Figures 6 and 7 that explicitly show the model differences from the observations). The models generally compare well with the observations in the representation of the latitude/depth distribution of high and low saturation waters. CanESM5 has a high saturation bias in low-latitude surface waters that is somewhat reduced in CanESM5-CanOE. Both CanESM5 models show a high saturation bias in Northern Hemisphere intermediate (e.g., 200-1000 m) depth waters that is larger than in the ensemble mean.

Taylor diagrams for a range of depths are shown for DIC in Figure 8 and for Ω_A in Figure 9 (for alkalinity, see Supplementary Figure S2). As expected, the MEM generally compares favourably with the individual models (e.g., Lambert and Boer, 2001). CanESM5 and CanESM5-CanOE compare favourably with the full suite of CMIP6 models. CanESM5-CanOE shows a gain in skill relative to CanESM5, and both show improvement relative to CanESM2. At 400 m, CanESM2 stands out as having extremely high variance, which is mostly due to extremely high DIC concentrations occurring over a limited area in the eastern equatorial Pacific (not shown).

https://doi.org/10.5194/gmd-2021-327
Preprint. Discussion started: 25 October 2021

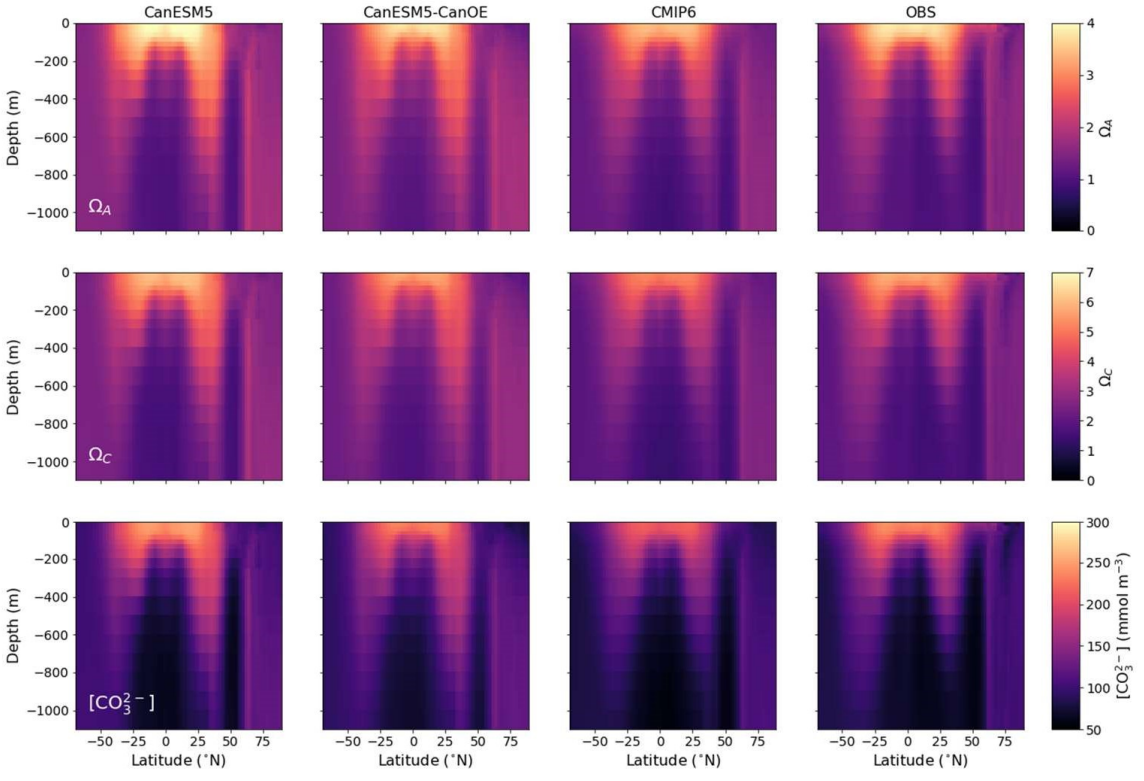

Figure 7 - Latitude-depth distribution of zonal mean (surface to 1150 m) aragonite saturation state (Ω_A), calcite saturation state (Ω_C), and carbonate ion concentration ([CO3--]) in mmol m^{-3} for CanESM5-CanOE, CanESM5, the mean for other CMIP6 models, and observations (GLODAP + WOA2013). Difference from the observation-based fields are shown in Supplementary Figure S3.

https://doi.org/10.5194/gmd-2021-327
Preprint. Discussion started: 25 October 2021

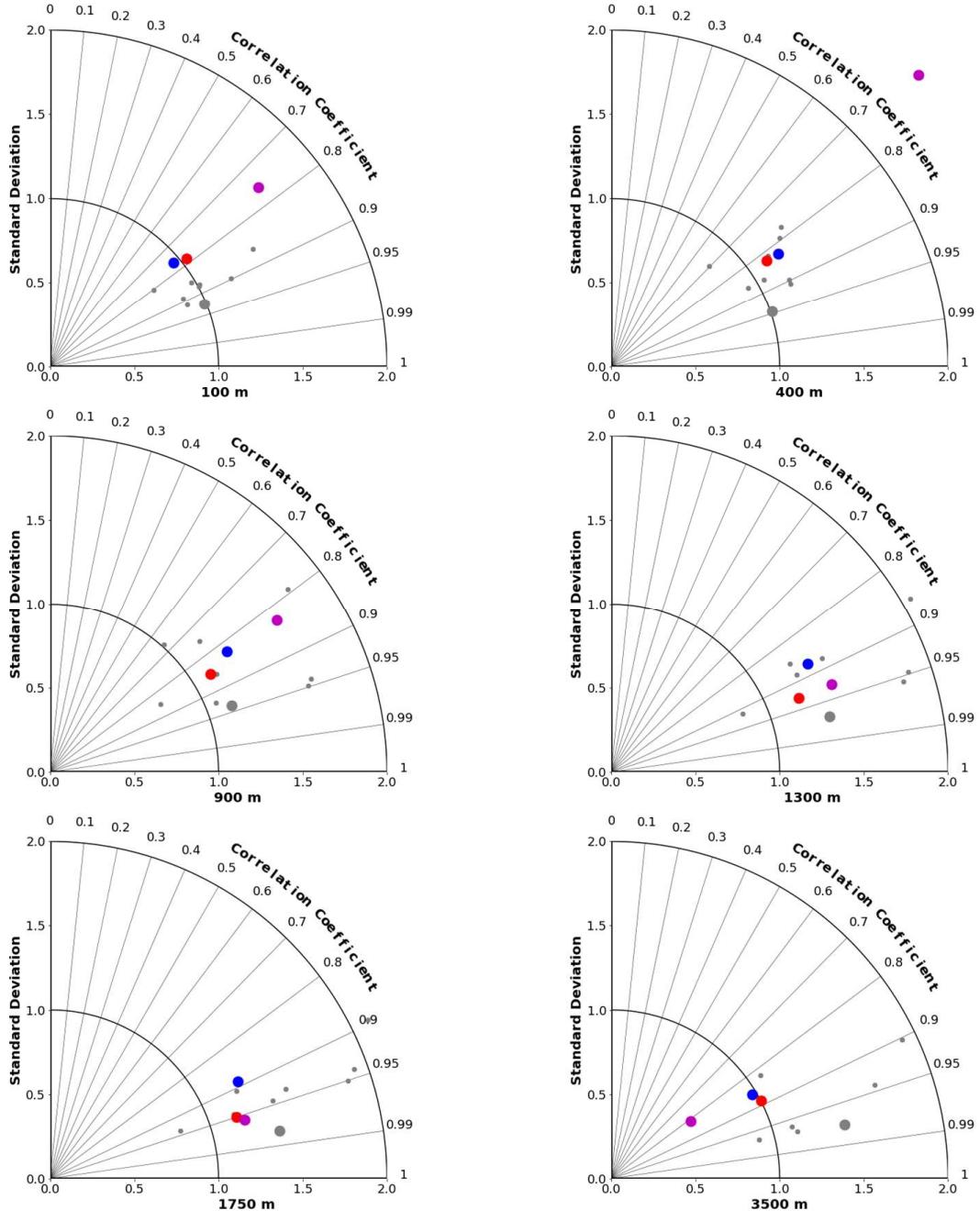

Figure 8 - Taylor diagrams comparing modelled and observed distributions of DIC at specific depths from 100 to 3500 m. Observations are from GLODAP (Lauvset et al., 2016). Red dots represent CanESM5-CanOE, blue dots CanESM5, magenta dots CanESM2, small grey dots other CMIP6 models, and large grey dots the model ensemble mean for all CMIP6 models except CanESM5 and CanESM5-CanOE.

https://doi.org/10.5194/gmd-2021-327
Preprint. Discussion started: 25 October 2021

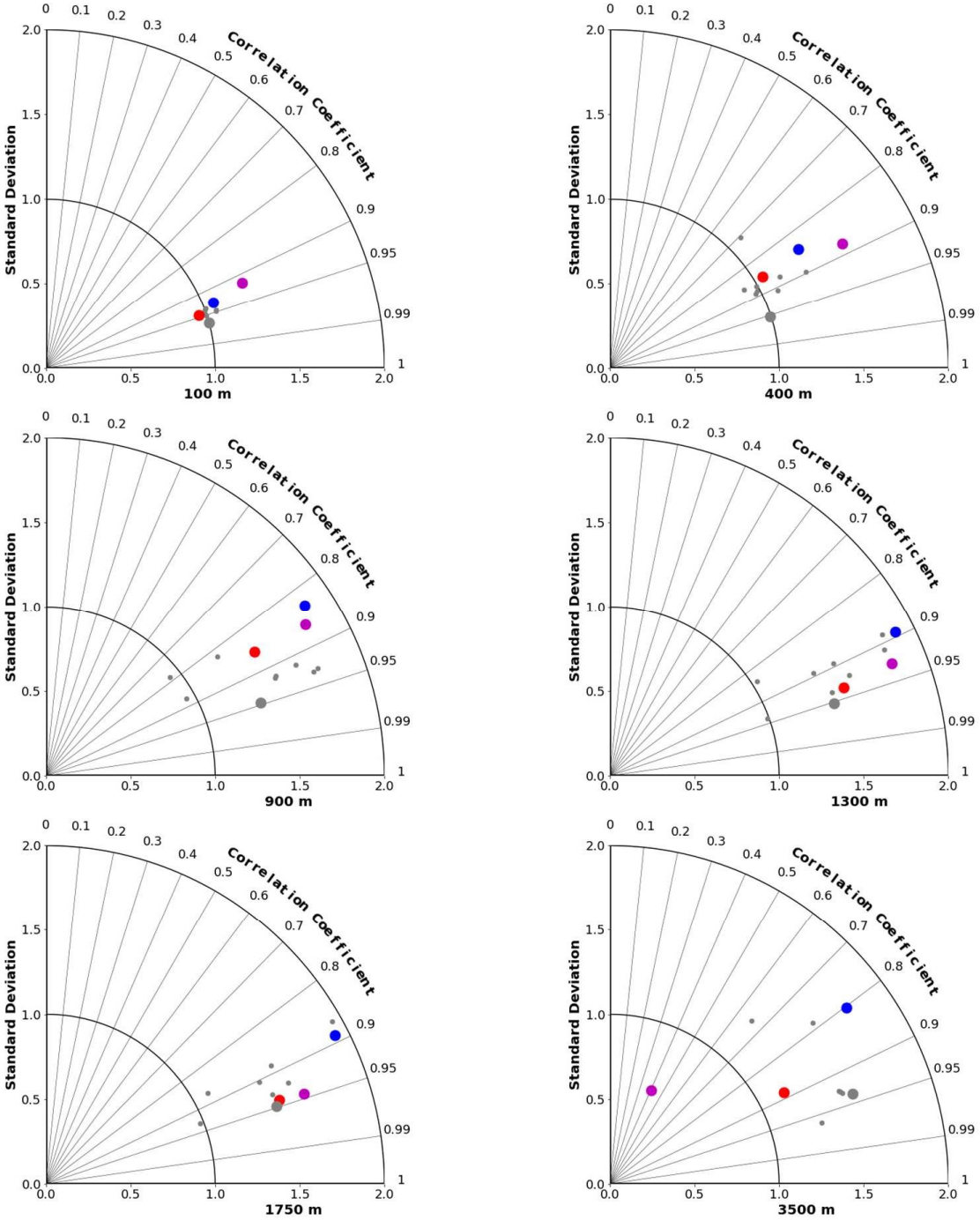

Figure 9 - Taylor diagrams comparing modelled and observed (GLODAP + WOA2013) distributions of Ω_A at specific depths from 100 to 3500 m. Symbol colours as in Figure 8.

https://doi.org/10.5194/gmd-2021-327
Preprint. Discussion started: 25 October 2021


Geoscientific Model Development Discussions

493 This bias is present in CanESM5 and in CMIP6 models generally (Figure 6) but involves much
494 lower concentrations spread over a larger area.
495
496 **3.3 N and Fe cycles**
497
498 An important difference between CMOC and CanOE is the inclusion of a prognostic Fe cycle.
499 The CMOC iron mask (Zahariev et al., 2008) was a pragmatic solution in the face of resource
500 limitations but is inherently compromised as it can not evolve with a changing climate. Other
501 centres that introduced a prognostic Fe cycle between CMIP5 and CMIP6 include JAMSTEC
502 (MIROC-ESM, MIROC-ES2L) and the UK Met Office (HadGEM2-ES, UKESM1-0-LL). The
503 first order test of a model with prognostic, interacting Fe and N cycles is whether it can
504 reproduce the distribution of High-Nutrient, Low-Chlorophyll (HNLC) regions and the
505 approximate surface macronutrient concentrations within these. CanESM5-CanOE succeeded by
506 this standard, although the surface nitrate concentrations are biased low in the subarctic Pacific
507 and equatorial Pacific and high in the Southern Ocean and in the global mean (Figure 10).
508
509 The seasonal cycle of the zonal mean surface nitrate concentration for a selection of CMIP6
510 models is shown in Figure 11. CanESM5, CanESM5-CanOE, and CNRM-ESM2-1 reproduce the
511 equatorial enrichment and the low concentrations in the tropical-subtropical latitudes fairly well.
512 Some models either have very weak equatorial enrichment (MPI-ESM1-2-LR) or too high a
513 concentration in the off-equatorial regions (UKESM1-0-LL, NorESM2-LM). UKESM1-0-LL
514 has very high concentrations throughout the low-latitude Pacific, which biases the ensemble
515 mean (Figure 11a). Figure 11b shows the same data as Figure 11a but for a more limited latitude

https://doi.org/10.5194/gmd-2021-327
Preprint. Discussion started: 25 October 2021

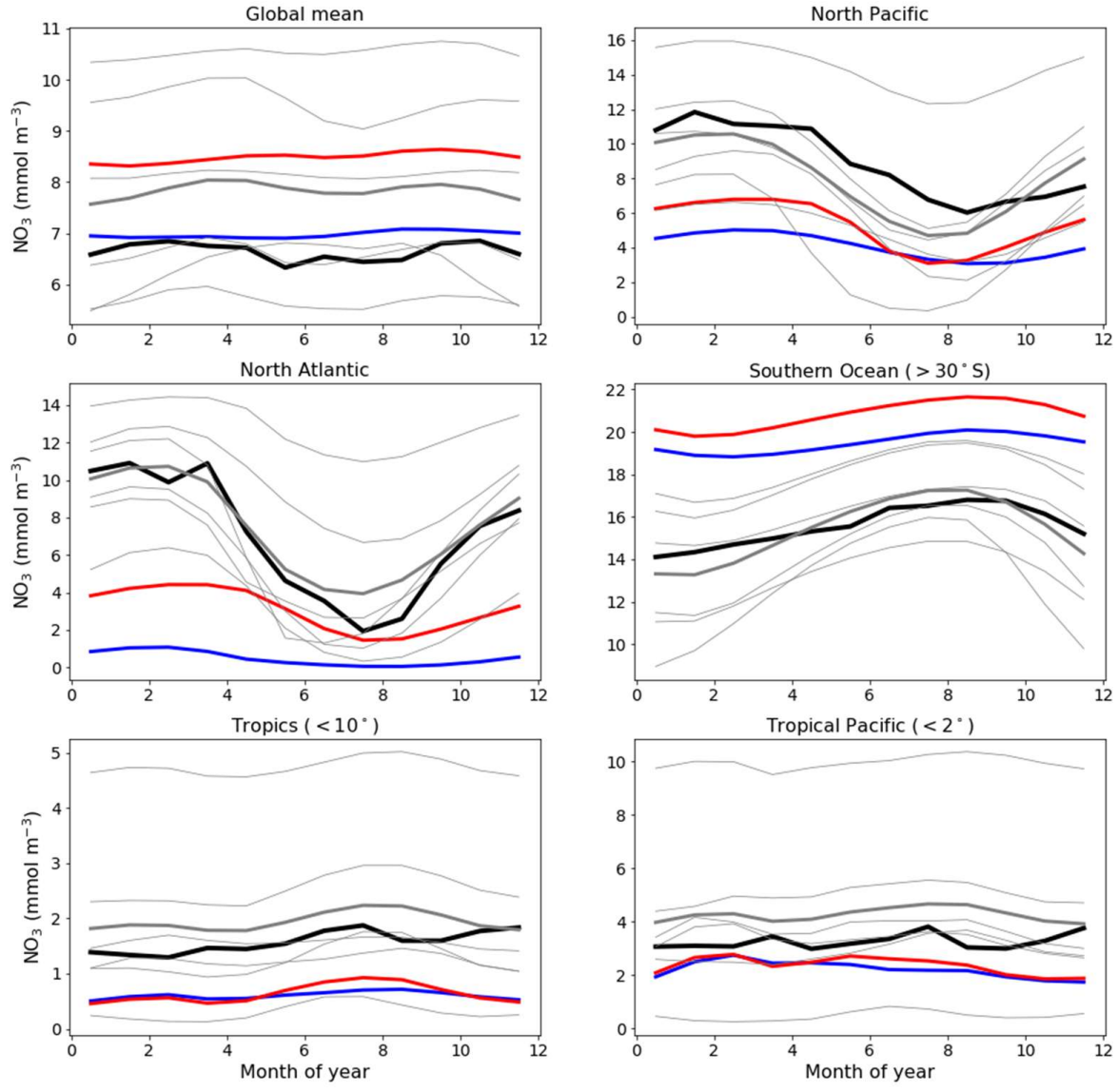

Figure 10 - Climatological seasonal cycle of surface nitrate concentration averaged for selected ocean regions. Thick red line represents CanESM5-CanOE, thick blue line CanESM5, thick black line observations (WOA2013), thin grey lines individual CMIP6 models, and thick grey line the model ensemble mean (excluding CanESM5 and CanESM5-CanOE). Regional boundaries are given in Supplementary Table S4.

https://doi.org/10.5194/gmd-2021-327
Preprint. Discussion started: 25 October 2021

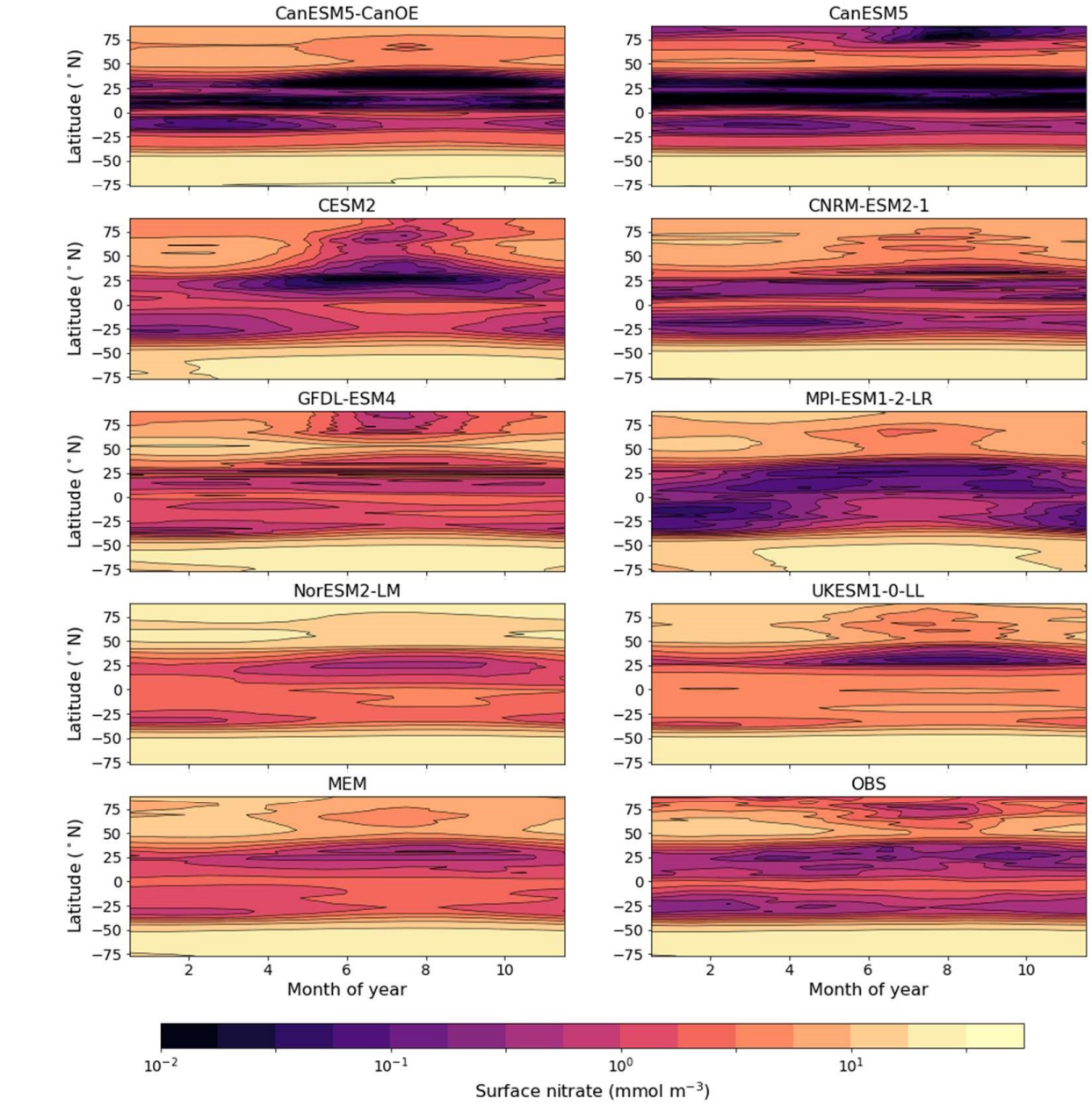

Figure 11 - (a) Climatological seasonal cycle of zonal mean surface nitrate concentration, for a selection of CMIP6 models, a model ensemble mean (MEM) excluding CanESM5 and CanESM5-CanOE, and an observation-based data product (WOA2013).

https://doi.org/10.5194/gmd-2021-327
Preprint. Discussion started: 25 October 2021

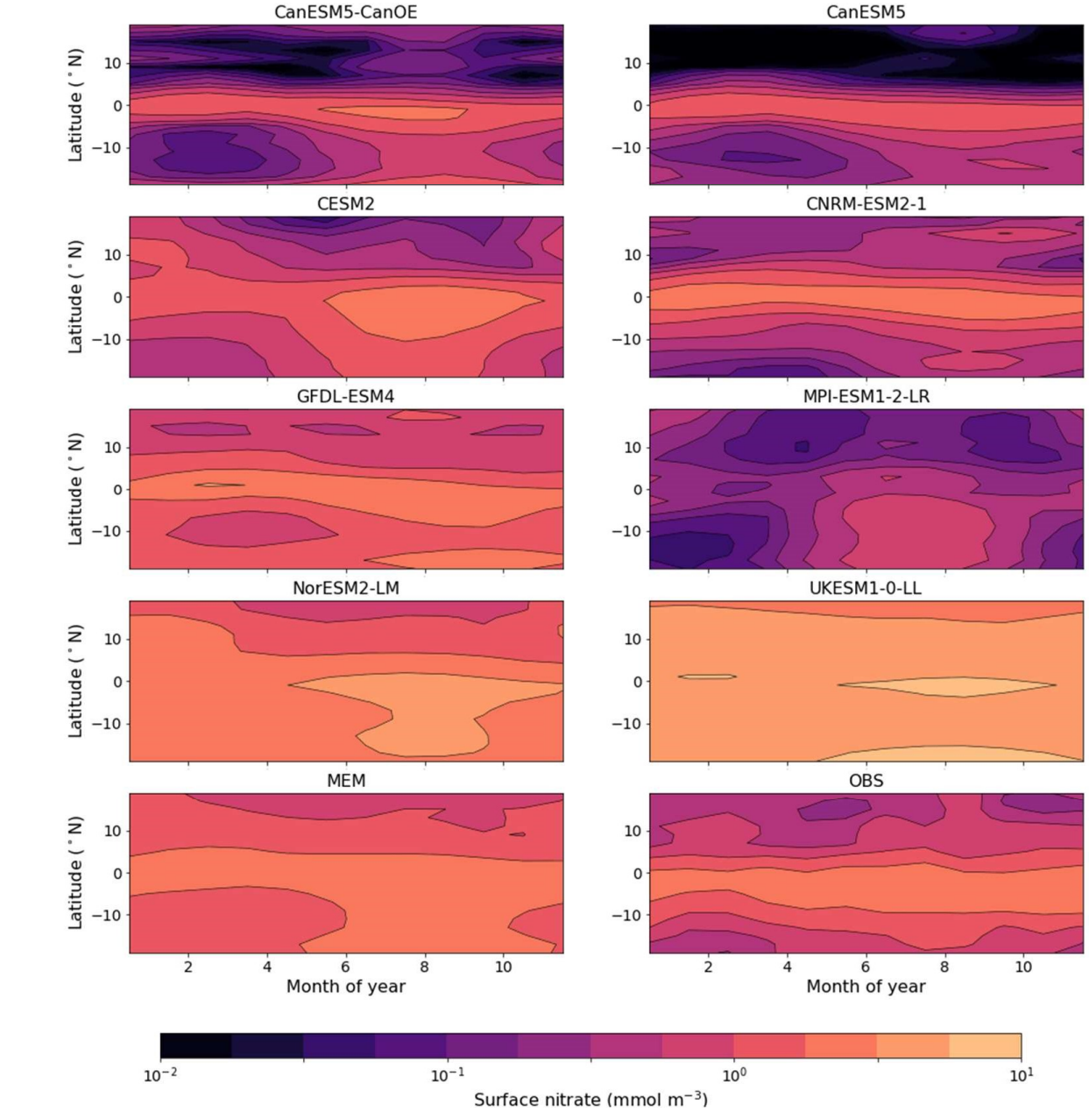

Figure 11 (b) As Figure 11(a) but for latitudes <20°.

https://doi.org/10.5194/gmd-2021-327
Preprint. Discussion started: 25 October 2021


Geoscientific Model Development Discussions

519 range to better illustrate model behaviour in the tropics. CanESM5, CanESM5-CanOE, and
520 CNRM-ESM2-1 reproduce the seasonal cycle of tropical upwelling (e.g., Philander and Chao,
521 1991), with highest concentrations in summer.
522
523 The surface distribution of dissolved iron (dFe) in various CMIP6 models is shown in Figure 12.
524 For Fe there is no observation-based global climatology with which to compare the model
525 solutions (some comparisons to available profile data are shown in Supplementary Figures S4b-
526 g). CanESM5-CanOE shows a similar overall spatial pattern to other models, and generally falls
527 in the middle of the spread, particularly regarding concentrations in the Southern Ocean. Several
528 models show extremely high concentrations in the tropical-subtropical North Atlantic (Sahara
529 outflow region). CanESM5-CanOE, along with CNRM-ESM2-1 and CESM2, has much less
530 elevated concentrations in this region, due to lower deposition or greater scavenging or both.
531 CanESM5-CanOE has its lowest concentration in the eastern subtropical South Pacific, which is
532 common to many models (Figure 12). The area of strong surface depletion is generally more
533 spatially restricted in CanESM5-CanOE than in other models, and surface dFe concentrations are
534 greater over large areas of the Pacific. Both the north-south and east-west asymmetry of
535 distribution in the Pacific is greater in CanESM5-CanOE than in most other models, some of
536 which show the South Pacific minimum extending westward across the entire basin, and others
537 into the Northern Hemisphere. Only in CESM2 is this minimum similarly limited to the
538 southeast Pacific.
539
540 The mean depth profiles of dFe are shown in Figure 13. Some models show more of a “nutrient-
541 type” (increasing with depth due to strong near-surface biological uptake and subsequent

https://doi.org/10.5194/gmd-2021-327
Preprint. Discussion started: 25 October 2021

Geoscientific Model Development Discussions
Open Access
EGU

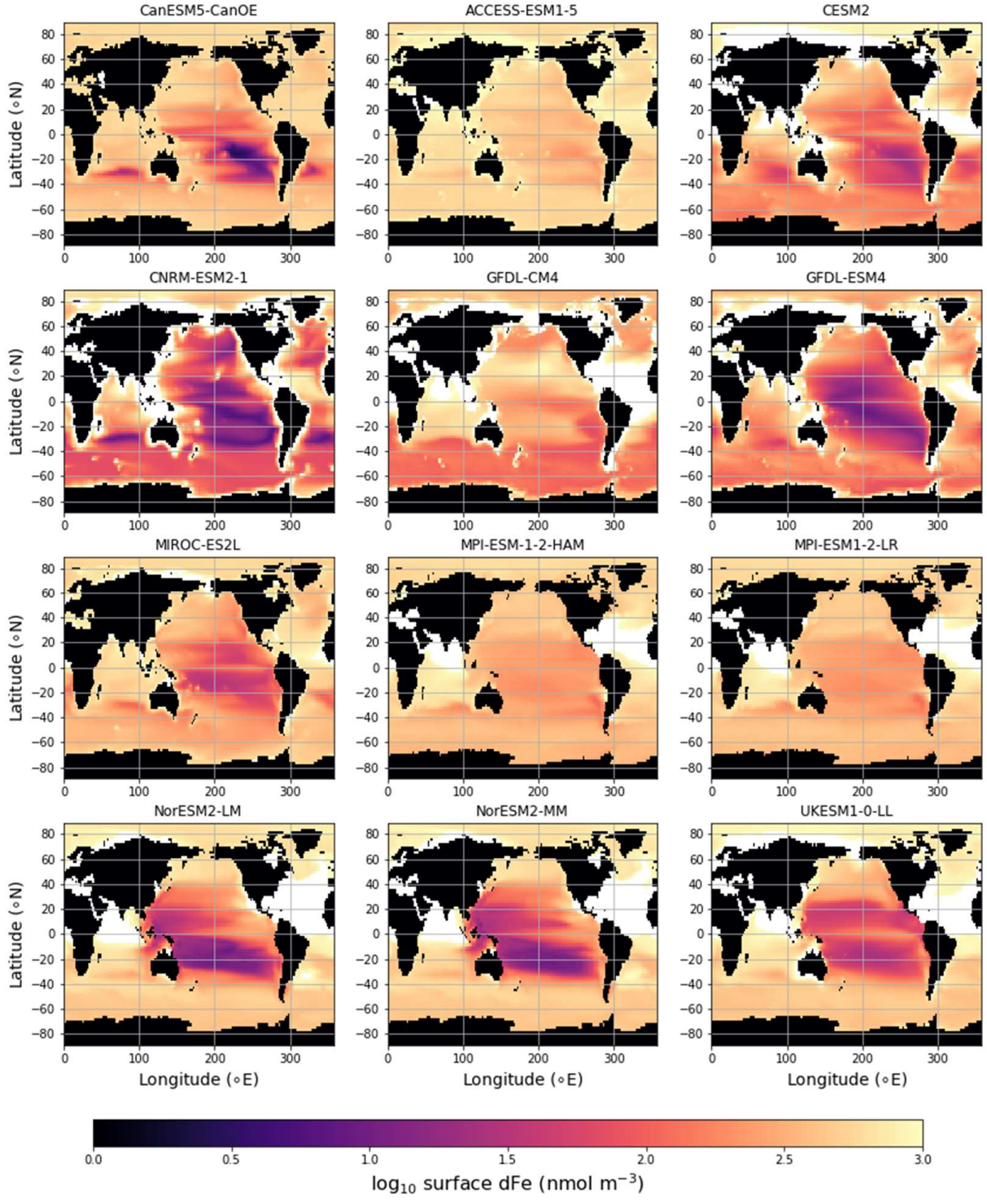

Figure 12 - Global distribution of dissolved iron (dFe) concentration (log10 of concentration in nmol m^{-3}) at the ocean surface for CanESM5-CanOE and other CMIP6 models that published this field. Concentrations exceeding 1000 nmol m^{-3} are masked white.

https://doi.org/10.5194/gmd-2021-327
Preprint. Discussion started: 25 October 2021

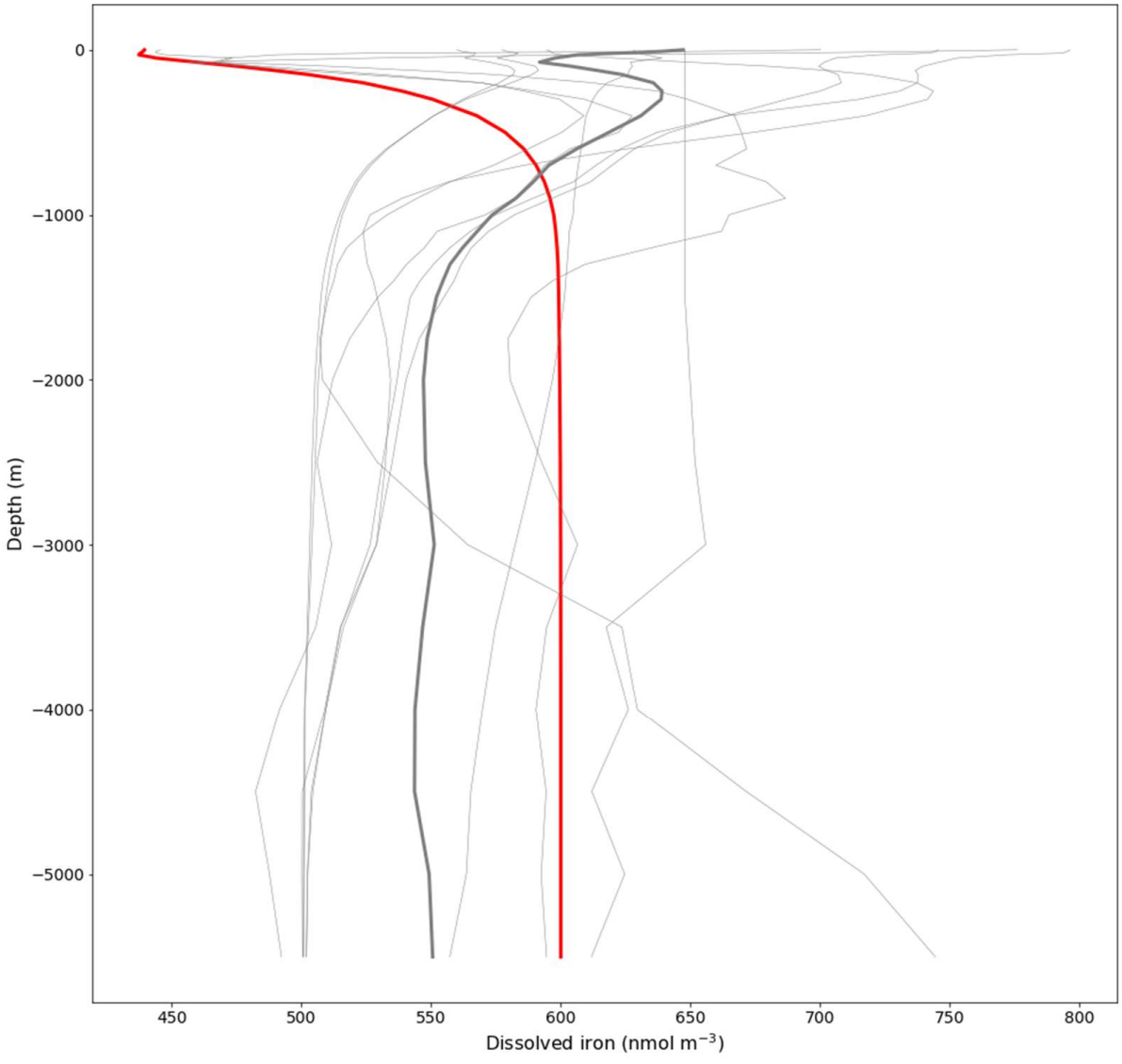

Figure 13 - Global mean depth profiles of dissolved iron concentration for CanESM5-CanOE and other CMIP6 models that published this field. GFDL-CM4 is excluded because it has very high concentrations (>2000 nmol m^{-3}) near the surface. Thick red line represents CanESM5-CanOE, thin grey lines individual CMIP6 models, and the thick grey line the model ensemble mean (excluding CanESM5-CanOE and GFDL-CM4).

https://doi.org/10.5194/gmd-2021-327
Preprint. Discussion started: 25 October 2021


Geoscientific Model Development Discussions

remineralization) profile, some a more "scavenged-type" (maximal at the surface, declining with depth) profile (cf. Li, 1991; Nozaki, 2001), and others a hybrid profile (increasing downward but with a surface enrichment). CanESM5-CanOE is at the "nutrient-type" end of spectrum with a generally monotonic increase with depth to a near-constant deep-water concentration of 0.6 nM and a very slight near-surface enrichment (see also Supplementary Figures S4b,c). In CanESM5-CanOE the scavenging model is very simple, with distinct regimes for concentrations greater or less than 0.6 nM; scavenging rates are very high above this threshold which causes deep-water concentrations to converge on this value. The generally nutrient-like profile suggest that in CanOE the scavenging rate is quite low for concentrations below 0.6 nM. CanOE considers particulate organic matter (POM) as an index of all particulate matter available for scavenging onto, and model POM concentrations fall off rapidly below the euphotic zone (not shown).

Mean surface nitrate and dFe concentrations for selected ocean regions are shown in Figure 14. CanESM5-CanOE shows concentrations that are within the range of CMIP6 models, although in some cases at the higher or lower end. Surface nitrate concentrations generally compare favourably with the observation-based climatology, but are biased low in HNLC regions other than the Southern Ocean. These biases are not necessarily a consequence of having too much or too little iron. For example, in the Southern Ocean CanESM5-CanOE has among the highest surface nitrate concentrations, but it also has some of the highest dFe concentrations, and the high nitrate bias is present in CanESM5 as well. Comparisons with the limited GEOTRACES data available suggest that near surface dFe concentrations in the Southern Ocean are biased high rather than low in CanESM5-CanOE (not shown). One region where there does seem to be a strong correlation between surface nitrate and dFe concentrations is the western subarctic

https://doi.org/10.5194/gmd-2021-327
Preprint. Discussion started: 25 October 2021

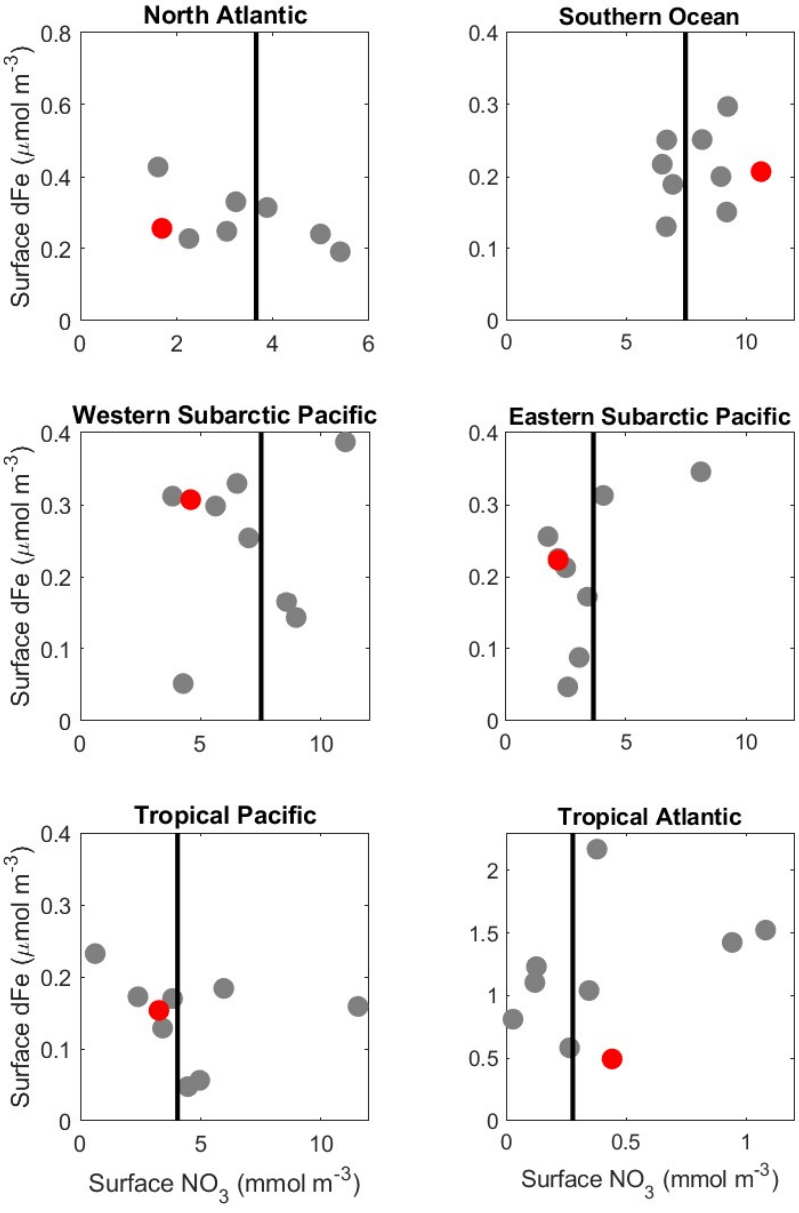

Figure 14 - Mean surface nitrate (NO_3) vs. dissolved iron (dFe) concentrations in different oceans, including the major high nutrient / low chlorophyll (HNLC) regions. CanESM5-CanOE is shown as a red dot and other CMIP5 models as grey dots (CanESM5 is not included because it does not have iron). Observed NO_3 is shown as a vertical black line as there are no observational estimates of dFe concentration. Region definitions are given in Supplementary Table S4.

https://doi.org/10.5194/gmd-2021-327
Preprint. Discussion started: 25 October 2021

Pacific. All but two models fall along a spectrum from high Fe / low nitrate to low Fe / high nitrate. CanESM5-CanOE falls near the high Fe / low nitrate end of the range.

Surface nitrate concentrations along the Pacific equator during the upwelling season (June-October) for CanESM5 and CanESM5-CanOE are shown in Figure 15. CanESM5-CanOE better represents the east-west gradient, while CanESM5 has slightly higher concentrations in the core upwelling region. Both models underestimate the highest concentrations around 100°W. Some localized maxima in this data product are due to undersampling; however, examination of ancillary data sets such as satellite sea surface temperature suggests that the enrichment at 100°W accurately reflects ocean upwelling (not shown). Although CanESM5 iron limitation is calculated from an earlier version of the same data product, the Fe mask is based on the minimum nitrate concentration over the annual cycle, whereas the data shown here are for the upwelling season. In CanESM5-CanOE, the distribution of surface nitrate is an emergent property of the model, and the fidelity to the observed distribution is generally good.

3.4 Plankton biomass, detritus, and particle flux

The relative abundance of the four living plankton groups are shown in Figure 16 for a range of ocean regions. Both CanESM models mostly compare favourably with observation-based estimates of phytoplankton biomass, except in the tropics where CanESM5-CanOE has very high biomass. Both CanESM models have low phytoplankton biomass in the North Atlantic. In the North Pacific and the Southern Ocean, CanESM5-CanOE reproduces the observation-based estimates well, and CanESM5 slightly less well. The general pattern is that large and small

https://doi.org/10.5194/gmd-2021-327
Preprint. Discussion started: 25 October 2021

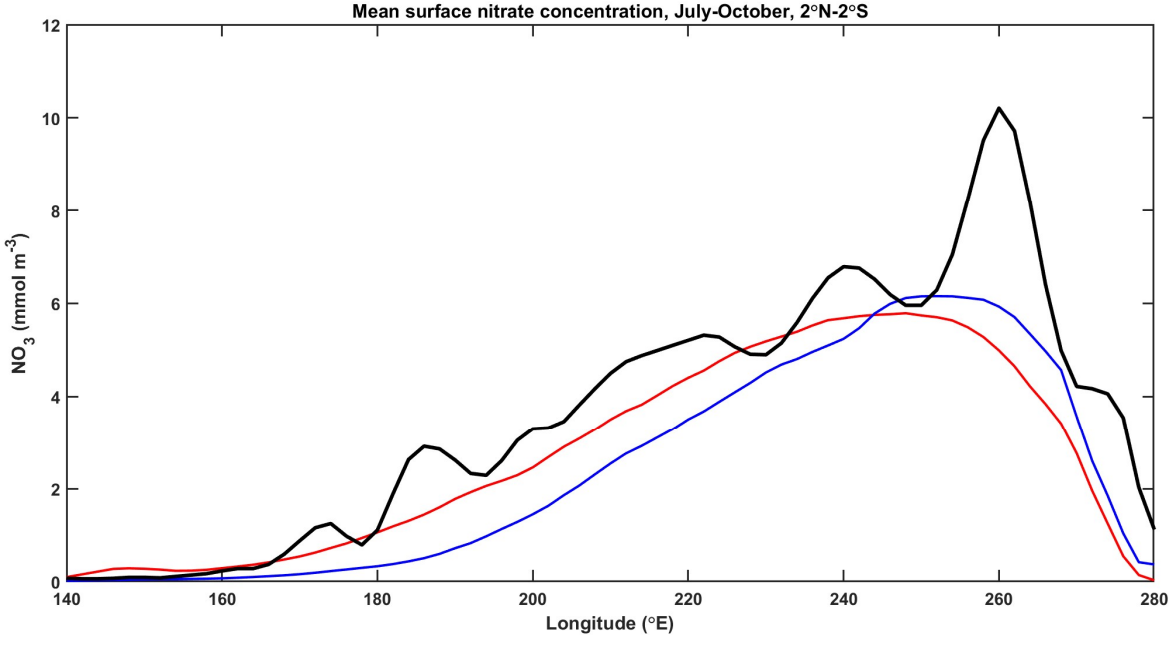

Figure 15 - Surface nitrate (NO3) concentrations along the Pacific equator (mean from 2°S-2°N) during the upwelling season (June-October) for CanESM5-CanOE (red), CanESM5 (blue), and WOA2013 observations (black).

https://doi.org/10.5194/gmd-2021-327
Preprint. Discussion started: 25 October 2021

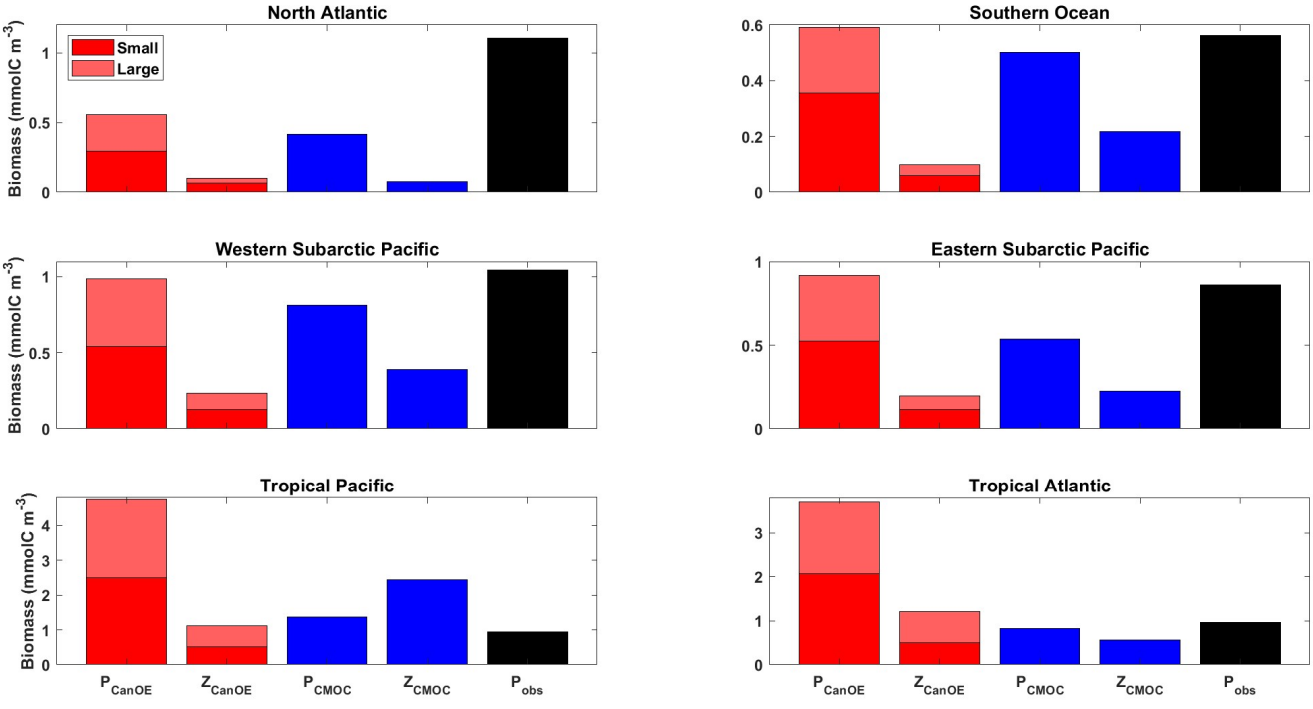

Figure 16 - Annual mean surface ocean concentration of large and small phytoplankton and zooplankton in CanESM5-CanOE (red) and of phytoplankton and zooplankton in CanESM5 (blue) for the representative ocean regions shown in Figure 14. Observational estimates (black) are for phytoplankton biomass calculated from satellite ocean colour estimates of surface chlorophyll (SeaWiFS/MODIS; Tesdal et al. 2016), assuming a carbon-to-chlorophyll ratio of 50 g/g. Region definitions are given in Supplementary Table S4.

https://doi.org/10.5194/gmd-2021-327
Preprint. Discussion started: 25 October 2021


Geoscientific Model Development Discussions

phytoplankton have similar abundance, and are substantially more abundant than zooplankton. Part of the rationale for multiple food chains is that they better represent the way that actual plankton communities adapt to different physical ocean regimes and therefore are better able to simulate distinct ocean regions with a single parameter set (e.g., Chisholm, 1992; Armstrong, 1994; Landry et al., 1997; Friedrichs et al., 2007). The expectation is that small phytoplankton will be more temporally stable and large phytoplankton will fluctuate more strongly between high and low abundances.

The mean annual cycles of surface chlorophyll largely conform to the expected pattern, e.g., in the North Atlantic and the western subarctic Pacific large phytoplankton are dominant in summer and much more variable over the seasons (Figure 17). Compared to observations, CanESM5 models underestimate the amplitude of the seasonal cycle in the North Atlantic and overestimate it in the North Pacific. CanESM5 shows a stronger and earlier North Atlantic spring bloom compared to CanESM5-CanOE; the observations are in between the two in terms of timing, and both models underestimate the amplitude (Figure 17). In the tropics, the seasonal cycle is weak. The tropical Atlantic shows the expected seasonal cycle but not the expected dominance of large phytoplankton in summer. These size-fractionation patterns are difficult to validate against observations. CanESM5-CanOE generally overestimates the total near surface chlorophyll in both the tropical Pacific and the tropical Atlantic.

Zooplankton biomass (especially microzooplankton) is also somewhat difficult to test against observations, but our model concentrations appear to be biased low. White et al. (1995), for example, show a transect of vertically resolved mesozooplankton abundance along 140°W in the

https://doi.org/10.5194/gmd-2021-327
Preprint. Discussion started: 25 October 2021

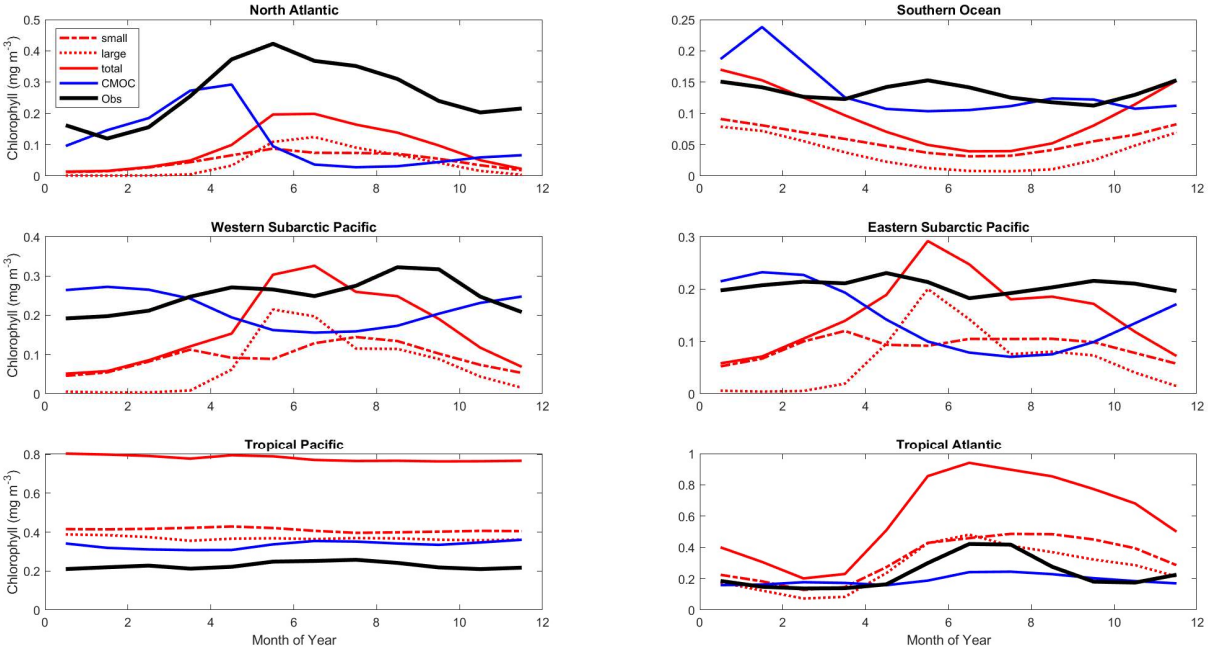

Figure 17 - Mean annual cycle of surface chlorophyll for the representative ocean regions shown in Figures 14 and 16. CanESM5-CanOE large and small phytoplankton concentrations are shown separately and combined (red) along with CanESM5 (blue) and observational estimates (black). Region definitions are shown in Supplementary Table S4.

https://doi.org/10.5194/gmd-2021-327
Preprint. Discussion started: 25 October 2021

617 tropical Pacific, with biomass ranging from about 0.1-0.7 mmolC m^3; CanESM5-CanOE
618 concentrations in this region are much lower. Stock et al. (2014) estimated depth-integrated
619 biomass of phytoplankton, mesozooplankton, and microzooplankton for a range of oceanic
620 locations in which intensive field campaigns have occurred (estimates of microzooplankton
621 biomass are relatively sparse). They found that in most locations phytoplankton and (combined)
622 zooplankton biomass are of comparable magnitude, whereas in CanESM5-CanOE zooplankton
623 biomass is consistently lower (Figure 16). The global integral biomass of mesozooplankton is
624 about an order of magnitude less than the 0.19 PgC estimated by Moriarty and O'Brien (2013).
625 The CanESM5 total of 0.14 Pg is relatively close to the Moriarty estimate but implicitly includes
626 microzooplankton.
627
628 Surface chlorophyll and POC for CanESM5-CanOE and for ocean colour observational data are
629 shown in Figure 18 (POC in the model is the sum of phytoplankton, microzooplankton, and
630 detrital carbon). The observations have a lower limit for POC that is not present in the model
631 (~17 mgC m^{-3}), which is unsurprising given the processes neglected in the model, i.e., in regions
632 of very low chlorophyll there is still substantial dissolved organic carbon, bacteria that consume
633 it, and microzooplankton that consume the bacteria and produce particulate detritus. The
634 observational data show a fairly linear relationship at low concentrations, but with a curvature
635 that implies a greater phytoplankton fraction in more eutrophic environments (cf. Chisholm,
636 1992). The model, by contrast, shows a fairly linear relationship over the whole range of
637 concentrations. In other words, the phytoplankton share of POC is higher and more constant in
638 the model than in the observations. The living biomass (phytoplankton + microzooplankton)
639 fraction of total POC in CanOE is generally in excess of 50% (not shown), which is implausible

https://doi.org/10.5194/gmd-2021-327
Preprint. Discussion started: 25 October 2021

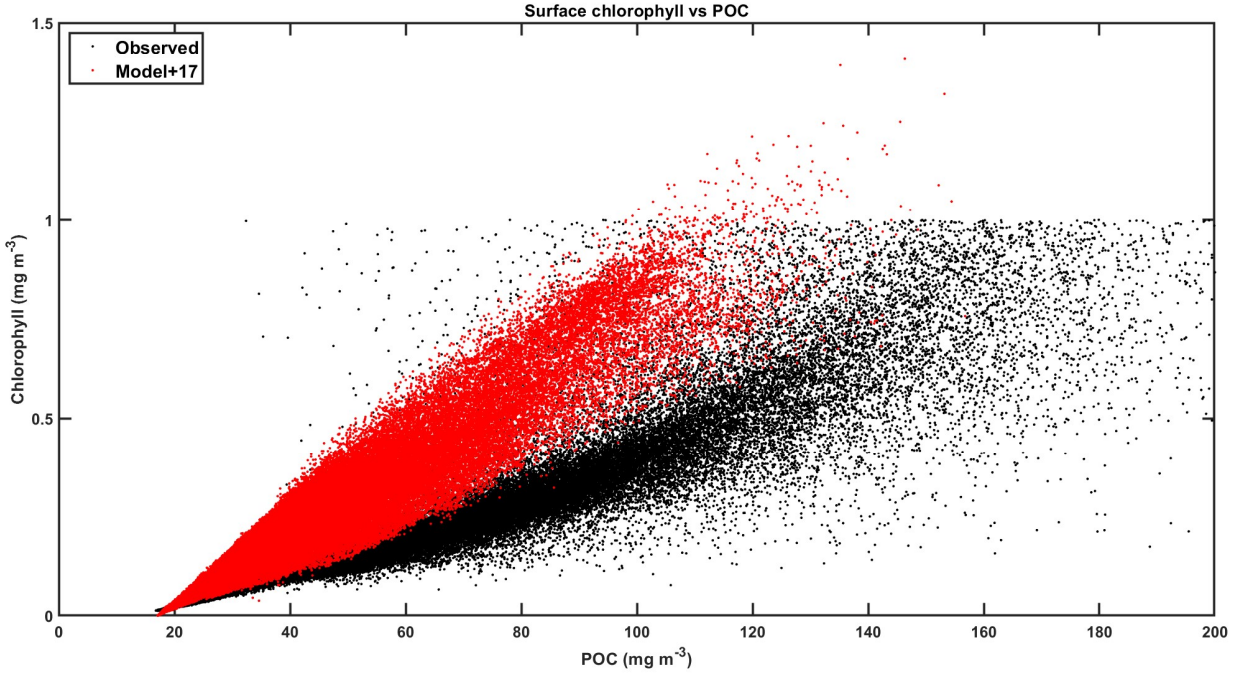

Figure 18 - Climatological surface particulate organic carbon (POC) vs. chlorophyll for CanESM5-CanOE (red) and observations (black). Data are for all ocean grid points (2x2° uniform global grid) for all months of the year where observational data are available. Model POC is offset 17 mg m^{-3} for illustrative purposes.

https://doi.org/10.5194/gmd-2021-327
Preprint. Discussion started: 25 October 2021

for a real-world oceanic microbial community (e.g., Christian and Karl, 1994) but consistent with the relatively low rates of export from the euphotic zone.

Export production for a range of CMIP6 models is shown in Figure 19a. CanESM5-CanOE is at the low end of the range. Observations are not shown because the range of observational estimates covers almost the entire range of the plot (e.g., Siegel et al., 2016). Note also that CanESM5 export is quite a bit lower than in CanESM2, which is relatively high for CMIP5 models (not shown). The difference between CanESM2 and CanESM5 is attributable primarily to different circulation, although the different initialization fields for nitrate might also play a small role. The lower rate in CanESM5-CanOE is consistent with the above results regarding plankton community structure (e.g., the concentration of detritus is generally low compared to living biomass), as well as the lower sinking rate for small detritus. The latitudinal distribution of export is shown in Figure 19b. CanESM5 shows very high export in the mid-latitudes of the Southern Ocean, similar to CanESM2 (not shown). Both CanESM5 models show latitudinal patterns consistent with the range of other models. CanESM5 has slightly greater export in the equatorial zone; in both CanESM models the equatorial enrichment attenuates very rapidly with latitude and the rates are low in the subtropics.

3.5 Historical trends

Cumulative ocean uptake of CO_2 is shown in Figure 20 for the historical experiment (1850-2014). CanESM models are biased low relative to observation based estimates (~145 PgC, see Friedlingstein et al., 2020) and the ensemble mean of other models (144 PgC, Figure 20), but fall

https://doi.org/10.5194/gmd-2021-327
Preprint. Discussion started: 25 October 2021

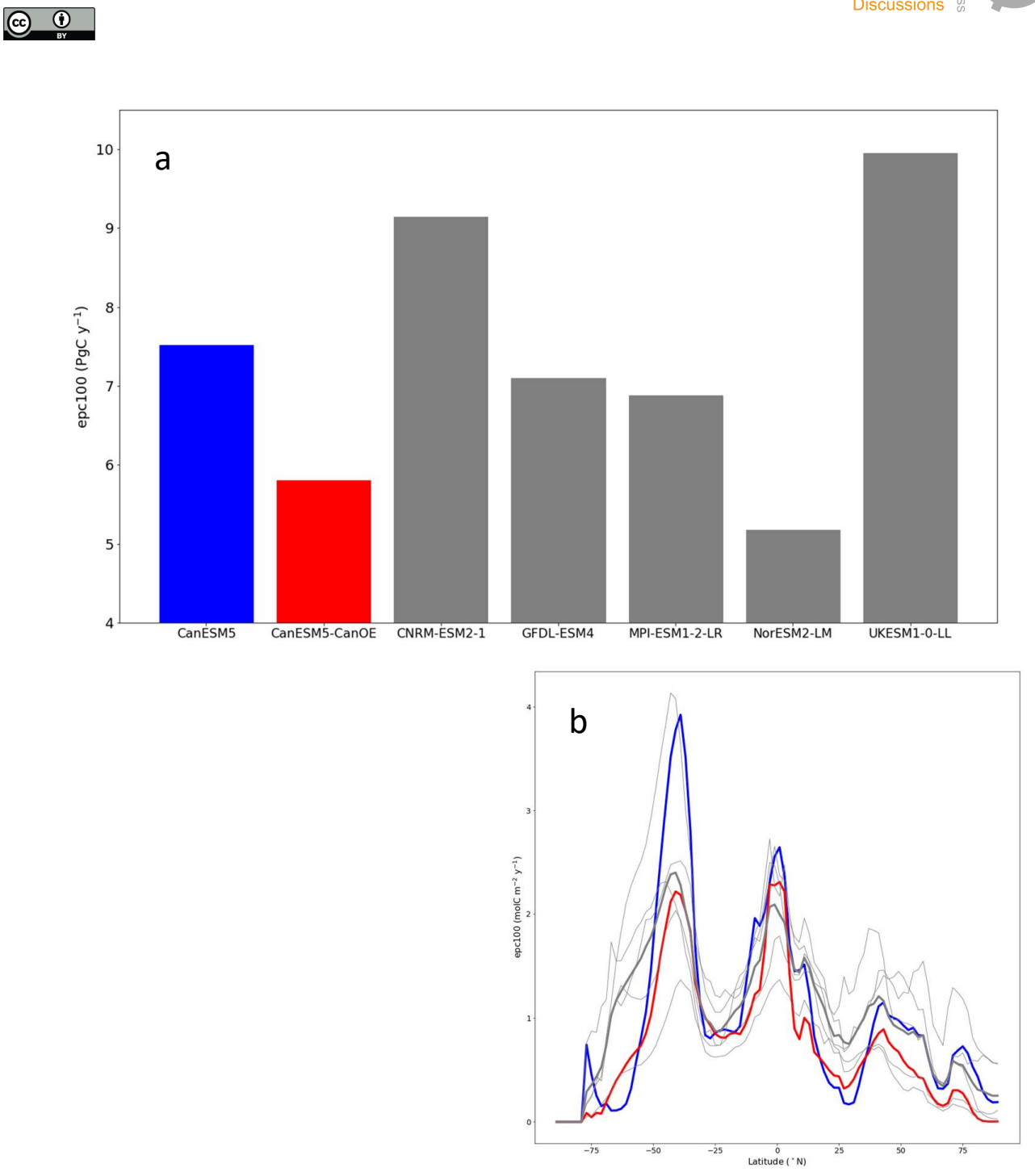

Figure 19 - (a) Global total export production (epc100) in PgC y^{-1} (b) and zonal mean export production in molC m^{-2} y^{-1} according to selected CMIP6 models (mean for 1985-2014 of historical experiment). Thick red line represents CanESM5-CanOE, thick blue line CanESM5, thin grey lines individual CMIP6 models, and thick grey line the model ensemble mean (excluding CanESM5 and CanESM5-CanOE).

https://doi.org/10.5194/gmd-2021-327
Preprint. Discussion started: 25 October 2021

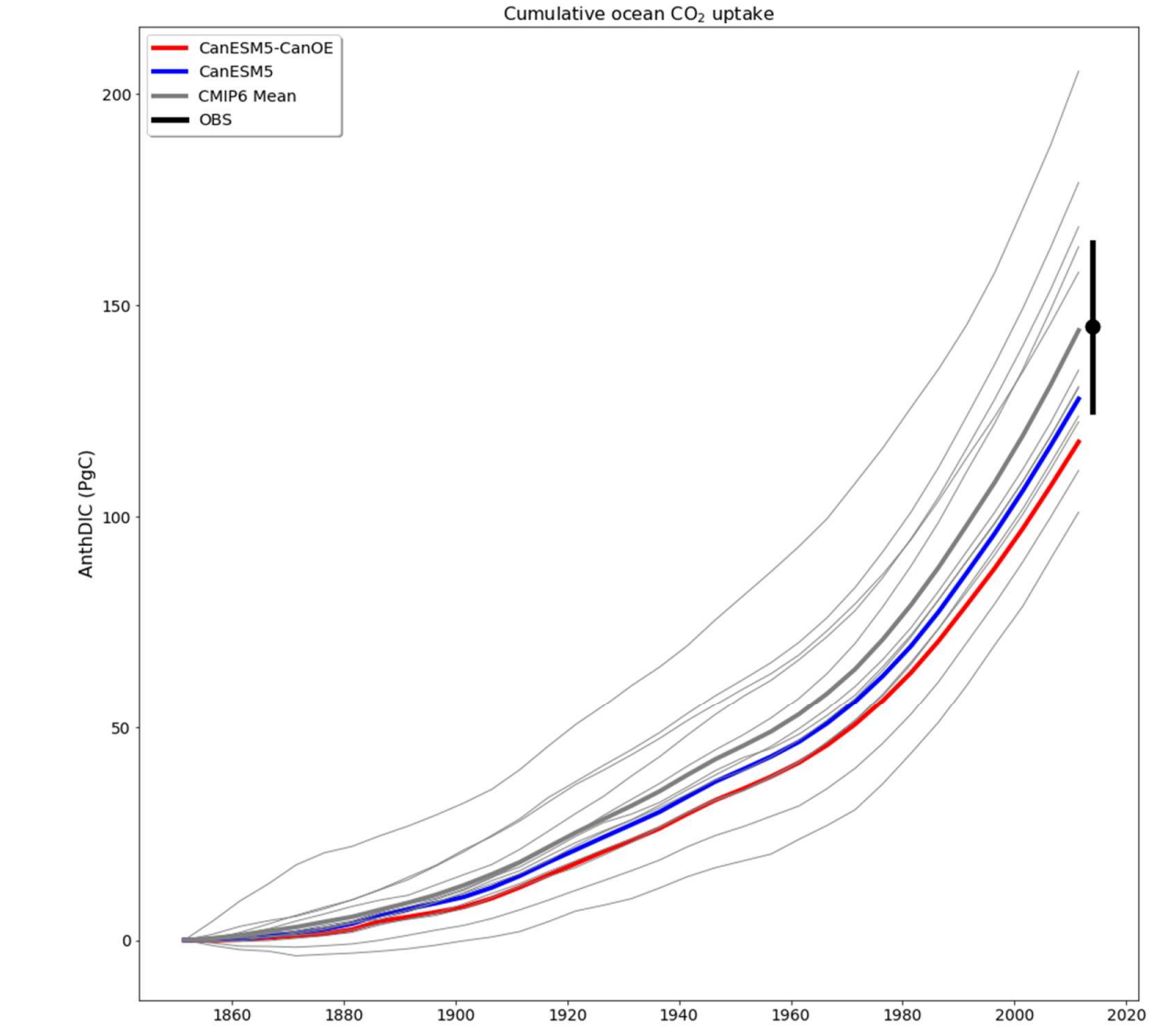

Figure 20 - Cumulative ocean uptake of carbon dioxide (CO_2) as anthropogenic dissolved inorganic carbon (AnthDIC) in PgC over the course of the historical experiment (1850-2014). Data are shown as successive five-year means. CMIP6 mean (thick grey line) indicates ensemble mean for CMIP6 models (thin grey lines) excluding CanESM5 (blue) and CanESM5-CanOE (red). An observation-based estimate of 145±20 PgC (Friedlingstein et al., 2020) is shown for nominal year 2014 (black).

https://doi.org/10.5194/gmd-2021-327
Preprint. Discussion started: 25 October 2021

well within the spread of CMIP6 models. CanESM5-CanOE has lower cumulative uptake than CanESM5 by ~ 10 PgC. As the models were not fully equilibrated when the historical run was launched, this difference does not necessarily arise from the biogeochemical model structure; part of the difference can be attributed to differences in the spinup protocol (cf. Séférian et al., 2016). The drift in the piControl experiment over the 165 years from the branching off of the historical experiment is -10.5 PgC in CanESM5-CanOE and -5.9 PgC in CanESM5, so drift accounts for about half (44%) of the difference in net ocean CO_2 uptake. The vertical distribution of anthropogenic DIC is very similar between CanESM5 and CanESM5-CanOE (not shown).

The long-term trend in global total export production is shown in Figure 21. The model values must be normalized in order to compare trends, since the differences among means are large compared to the changes over the historical period (Figure 19). CanESM5 shows a greater decline than most other CMIP6 models, while CanESM5-CanOE is more similar to non-CanESM models. Such trends are difficult or impossible to meaningfully constrain with observations, but the general expectation has been that export will decline somewhat due to increasing stratification (e.g., Steinacher et al., 2010). The change in CanESM5 is geographically widespread and not concentrated in a specific region or regions: export is maximal in the tropics and the northern and southern mid-latitudes (Figure 19b) and declines over the historical period in all of these regions (Supplementary Figure S1). In CanESM5-CanOE, export declines in the same regions, but the magnitude of the change is smaller, and in the Southern Ocean increases and decreases in different latitude bands largely offset each other.

https://doi.org/10.5194/gmd-2021-327
Preprint. Discussion started: 25 October 2021

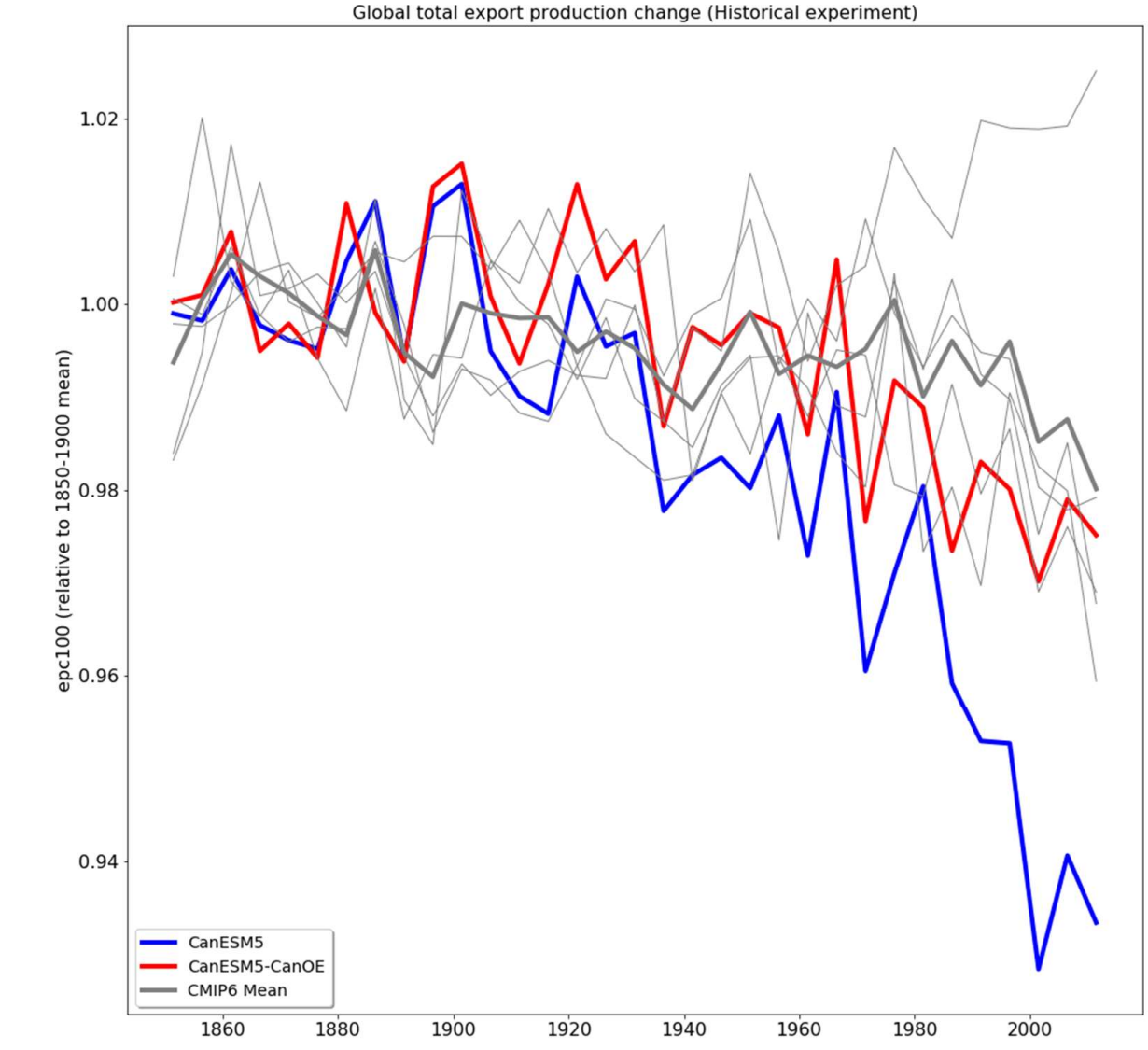

Figure 21 - Change in export production (epc100) over the course of the historical experiment (1850-2014), normalized to the 1850-1900 mean. Data are shown as successive five-year means. Thick red line represents CanESM5-CanOE, thick blue line CanESM5, thin grey lines other CMIP6 models, and thick grey line the ensemble mean of non-CanESM models.

https://doi.org/10.5194/gmd-2021-327
Preprint. Discussion started: 25 October 2021


Geoscientific Model Development Discussions

690 The trend in the volume of ocean water with O_2 concentration less than 6 or 60 mmol m^{-3} is
691 shown in Figure 22. Again, the totals are normalized to a value close to the preindustrial, as the
692 differences among models are large (Figure 5). For the volume with <60 mmol m^{-3}, CanESM
693 models show relatively little change; in CanESM5 the volume actually declines slightly, while in
694 CanESM5-CanOE it increases, but the total change is <1% in each case. As with the baseline
695 volumes, the range among models is large, with one model showing an increase approaching
696 10% of the total volume estimated for WOA2013 (Figures 5b and 22b). For the volume with <6
697 mmol m^{-3} (Figure 22a), CanESM models are among the most stable over time. In CanESM5, the
698 volume again declines, although this is within the range of internal variability. Again some
699 models show fairly large excursions, but in this case none shows a strong secular trend over the
700 last half-century.
701
702 **4. Discussion**
703
704 The development of CanOE was undertaken in response to some of the most severe limitations
705 of CanESM1/2, and in light of our collective experience. In addition to CMOC (Zahariev et al.,
706 2008), previous models developed by members of our group include Denman and Peña (1999;
707 2002), Christian et al. (2002a; 2002b), Christian (2005), and Denman et al. (2006). Christian et
708 al. (2002a) had a prognostic Fe cycle and multiple phytoplankton and zooplankton species, but
709 had fixed elemental ratios. Christian (2005) incorporated a cellular-regulation model, but only
710 for a single species and without Fe limitation. Christian (2005) had prognostic chlorophyll
711 whereas Denman and Pena (1999; 2002) and Christian et al. (2002a) used an irradiance-depend
712

https://doi.org/10.5194/gmd-2021-327
Preprint. Discussion started: 25 October 2021

Geoscientific Model Development Discussions

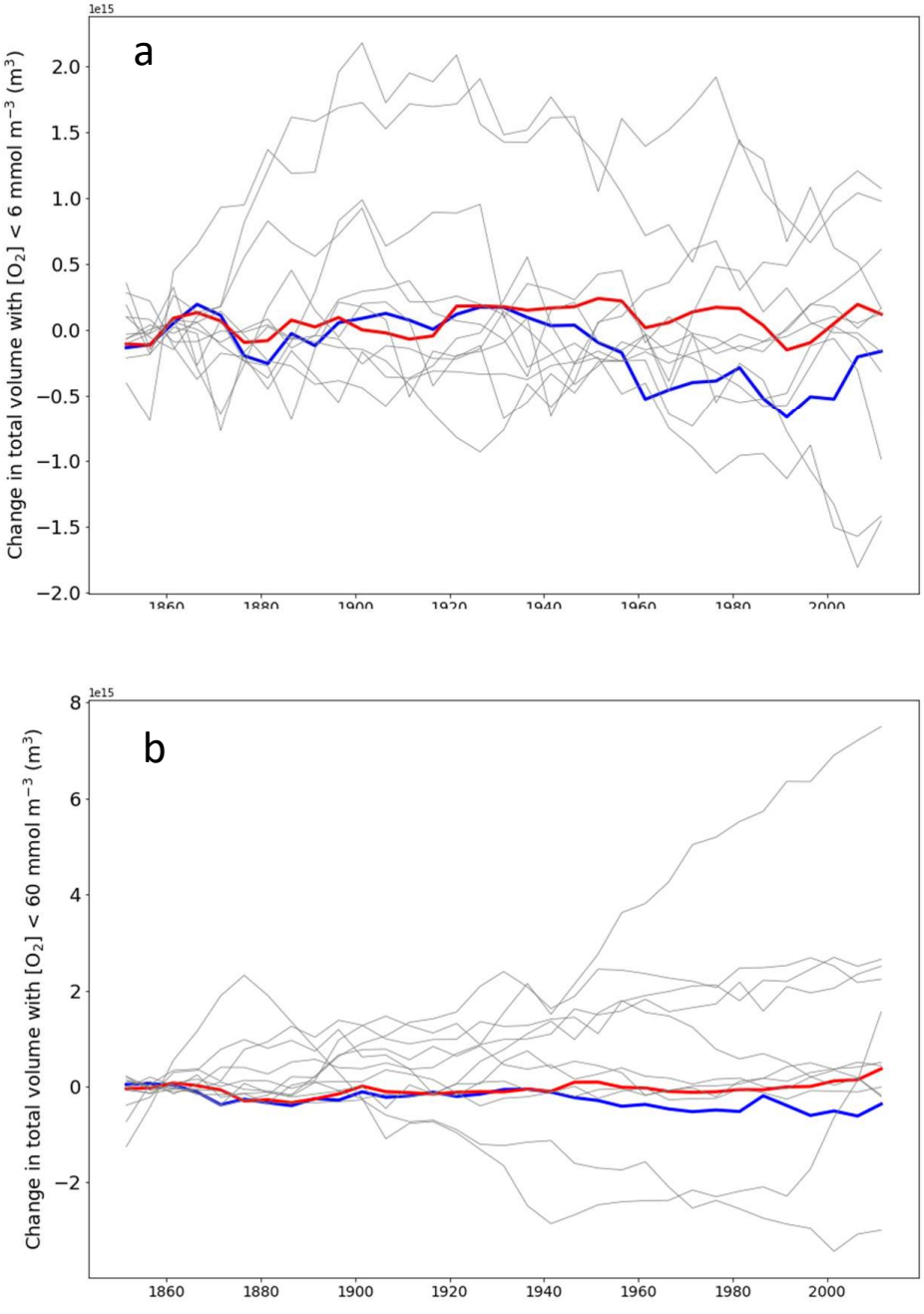

Figure 22 - (a) Change in total ocean volume with oxygen (O_2) concentration less than (a) 6 mmol m^{-3} and (b) 60 mmol m^{-3} over the course of the historical experiment (1850-2014), normalized to the 1850-1870 mean. Data are shown as successive five-year means. Thick red line represents CanESM5-CanOE, thick blue line CanESM5, and thin grey lines other CMIP6 models.

https://doi.org/10.5194/gmd-2021-327
Preprint. Discussion started: 25 October 2021


Geoscientific Model Development Discussions

ent diagnostic formulation. Christian et al. (2002a) used multiplicative (Franks et al., 1986) grazing, which creates stability in predator-prey interactions but severely limits phytoplankton biomass accumulation under nutrient-replete conditions.

One of the most important lessons from Christian et al. (2002a; 2002b) was that when a fixed Fe/N ratio is employed, sensitivity to this parameter is extreme. Because Fe cell quotas are far more variable than N, P, or Si quotas, treating this parameter as constant results in the specified value influencing the overall solution far more than any other parameter. CanESM5-CanOE largely succeeded in creating a prognostic Fe-N limitation model that produces HNLC conditions in the expected regions (Figures 10, 11, 14, 15), although surface nitrate concentration is low relative to observation-based estimates in some cases. External Fe sources and scavenging parameterizations will be revisited and refined in future versions. We note that the aeolian mineral dust deposition field employed here is derived from the CanESM atmosphere model; these processes are not presently interactive but could be made so in the future.

A particular issue with CanESM2 was that extremely high concentrations of nitrate occurred under the Eastern Boundary Current (EBC) upwelling regions. This error resulted from spreading denitrification out over the ocean basin so that introduction of new fixed N from N_2 fixation would balance denitrification losses within each vertical column, whereas in the real world denitrification is highly localized in the low oxygen environments under the EBCs. CanESM2 did not include oxygen, but CanESM5 CMOC incorporates oxygen as a 'downstream' tracer that does not feed back on other biogeochemical processes. The incorporation of a more process-based de-

https://doi.org/10.5194/gmd-2021-327
Preprint. Discussion started: 25 October 2021


Geoscientific Model Development Discussions

nitrification parameterization in CanOE is independent of the many other processes that are present in CanOE but not in CMOC: a CMOC-like model with prognostic denitrification is clearly an option. We chose not to include explicit, oxygen-dependent denitrification in CanESM5 because we wanted to maintain a CMOC-based model as close to the CanESM2 version as possible, and because oxygen would not then be a downstream tracer that does not affect other processes.

CanOE for the most part successfully reproduces the overall distribution of major tracers such as nitrate, oxygen, DIC and alkalinity (and dFe, to the extent that its distribution is known). One could argue that the gains made relative to CMOC are incremental. However, it is also important to note that CanOE explicitly simulates important processes that are highly parameterized or specified in CMOC. For example, the maintenance of HNLC regions is hardwired into CMOC by specifying iron limitation as a function of the present-day observed distribution of surface nitrate. Both models show substantial gains in skill relative to CanESM2. These gains are similar in the two models and in coupled or ocean only (with CanESM2 forcing) mode (not shown) and are, therefore, attributable primarily to improvements in the ocean circulation model, although differences in initialization and spinup may also play a small role (e.g., Séférian et al., 2016).

Plankton community structure in CanOE is somewhat biased toward high concentrations of phytoplankton, low concentrations of zooplankton and detritus, and low export (Sect. 3.4). In the development phase, a fair number of experiments were conducted with various values of the grazing rates and detritus sinking speeds. A wide range of values of these parameters was tested, with no resulting improvement in the overall results. Possibly the detrital remineralization rates are

https://doi.org/10.5194/gmd-2021-327
Preprint. Discussion started: 25 October 2021

too high, although primary production is also on the low end of the CMIP6 range (not shown), and would probably decline further if these rates were decreased. The model was designed around the Armstrong (1994) hypothesis of 'supplementation' vs 'replacement', i.e., small phytoplankton and their grazers do not become much more abundant in more nutrient-rich environments but rather stay at about the same level and are joined by larger species that are absent in more oligotrophic conditions (see also Chisholm, 1992; Landry et al., 1997; Friedrichs et al., 2007). The results presented here suggest that this was partially achieved but further improvement is possible (Figure 17).

As to whether the gains in skill with CanOE justify the extra computational cost, Taylor diagrams (Figures 4, 8, 9, and Supplementary Figure S2) show a modest but consistent gain across variables and depths, especially for alkalinity at mid-depths (Supplementary Figure S2), for which CanEM5 displays the least skill relative to other fields or depths. Other processes that are highly parameterized in CMOC, such as calcification and $CaCO_3$ dissolution, were not addressed in detail in this paper, but are an important factor in determining the subsurface distribution of alkalinity. As noted above for maintenance of HNLC conditions, we emphasize that we are simulating as an emergent property something that is parameterized in CMOC, and doing at least as well in terms of model skill. As a general rule, the potential for improving skill and achieving better results in novel environments (e.g., topographically complex regional domains like the Arctic Ocean and the boreal marginal seas), is expected to be greater in less parameterized models (e.g., Friedrichs et al., 2007; Tesdal et al., 2016).

https://doi.org/10.5194/gmd-2021-327
Preprint. Discussion started: 25 October 2021


Geoscientific Model Development Discussions

An updated version of CMOC with prognostic denitrification is clearly possible. However, for the reasons discussed above, a prognostic Fe cycle with a fixed phytoplankton Fe/N remains problematic, and the model would still have a single detritus sinking speed and remineralization length scale. We are also developing CanOE for regional downscaling applications (Hayashida, 2018; Holdsworth et al., 2021), and it is likely that the simplification of having a single particle sinking speed is not well suited to a domain with complex topography and prominent continental shelf and slope. The number of tracers in CanOE is not particularly large compared with other CMIP6 models. We expect to further refine CanOE and its parameterizations, evaluate it against new and emerging ocean data sets (e.g., GEOTRACES, biogeochemical ARGO), and incrementally improve CMOC (which we will maintain for a wide suite of physical-climate experiments for which ocean biogeochemistry is not central to the purpose). For CMIP6, we chose to keep CMOC as close to the CanESM2 version as possible. This strategy allows us to quantify how much of the improvement in model skill is due to the physical circulation, which is in fact substantial (e.g., Figure 8). The CanESM terrestrial carbon model is also undergoing important new developments (e.g., Asaadi and Arora, 2021) and we expect CanESM to continue to offer a credible contribution to global carbon cycle studies, as well as advancing regional downscaling and impacts science.

Code availability. The full CanESM5 source code is publicly available at gitlab.com/cccma/canesm; within this tree the CMOC/CanOE code can be found at gitlab.com/cccma/cannemo/-/tree/v5.0.3/nemo/CONFIG/CCC_CANCPL_ORCA1_LIM_CMOC or CCC_CANCPL_ORCA1_LIM_CANOE (last access: 21 September 2021). The version of the code which can be used to produce all the simulations submitted to CMIP6, and described in this

https://doi.org/10.5194/gmd-2021-327
Preprint. Discussion started: 25 October 2021


Geoscientific Model Development Discussions

804 paper, is tagged as v5.0.3 and has the associated DOI: https://doi.org/10.5281/zenodo.3251113
805 (Swart et al., 2019b).
806
807 *Data availability*. All CanESM5 simulations conducted for CMIP6, including those described in
808 this paper, are publicly available via the Earth System Grid Federation (ESGF). All observational
809 data and other CMIP6 model data used are publicly available.
810
811 *Author contributions.* Formulation of the overall research goals and aims: JRC, KLD, NS, NCS;
812 Implementation and testing of the model code: JRC, HH, AMH, WGL, OGJR, AES, NCS; Car-
813 rying out the experiments: JRC, WGL, OGJR, AES, NCS; Creation of the published work: JRC,
814 HH, AMH, AES, NS, NCS.
815
816 *Competing interests*. The authors declare that they have no conflict of interest.
817
818 *Disclaimer*. CanESM has been customized to run on the ECCC high-performance computer, and
819 a significant fraction of the software infrastructure used to run the model is specific to the indi-
820 vidual machines and architecture. While we publicly provide the code, we cannot provide any
821 support for migrating the model to different machines or architectures.
822
823 *Acknowledgments*. This work was made possible by the combined efforts of the CCCMa model
824 development team and computing support team. We thank the data contributors to and develop-
825 ers of the observation-based data products, the NASA ocean colour team, and all of the CMIP6

https://doi.org/10.5194/gmd-2021-327
Preprint. Discussion started: 25 October 2021


Geoscientific Model Development Discussions

data contributors. The Python packages mocsy by Jim Orr and SkillMetrics by Peter Rochford were invaluable tools in the analysis. William Merryfield and Andrew Ross made useful comments on an earlier draft. This paper is dedicated to the memory of Mr. Fouad Majaess, who supported CCCMa supercomputer users for many years and passed away suddenly in 2020.

Literature Cited

Arguez, A. and Vose, R.: The Definition of the Standard WMO Climate Normal The Key to Deriving Alternative Climate Normals, Bulletin of the American Meteorological Society, 92, 699-704, 10.1175/2010BAMS2955.1, 2011.

Armstrong, R.: Grazing limitation and nutrient limitation in marine ecosystems - steady-state solutions of an ecosystem model with multiple food-chains, Limnology and Oceanography, 39, 597-608, 1994.

Arora, V., Scinocca, J., Boer, G., Christian, J., Denman, K., Flato, G., Kharin, V., Lee, W., and Merryfield, W.: Carbon emission limits required to satisfy future representative concentration pathways of greenhouse gases, Geophysical Research Letters, 38, 10.1029/2010GL046270, 2011.

Arora, V., Boer, G., Christian, J., Curry, C., Denman, K., Zahariev, K., Flato, G., Scinocca, J., Merryfield, W., and Lee, W.: The Effect of Terrestrial Photosynthesis Down Regulation on the Twentieth-Century Carbon Budget Simulated with the CCCma Earth System Model, Journal of Climate, 22, 6066-6088, 10.1175/2009JCLI3037.1, 2009.

Asaadi, A. and Arora, V.: Implementation of nitrogen cycle in the CLASSIC land model, Biogeosciences, 18, 669-706, 10.5194/bg-18-669-2021, 2021.

Aumont, O., Ethe, C., Tagliabue, A., Bopp, L., and Gehlen, M.: PISCES-v2: an ocean biogeochemical model for carbon and ecosystem studies, Geoscientific Model Development, 8, 2465-2513, 10.5194/gmd-8-2465-2015, 2015.

Babbin, A., Keil, R., Devol, A., and Ward, B.: Organic Matter Stoichiometry, Flux, and Oxygen Control Nitrogen Loss in the Ocean, Science, 344, 406-408, 10.1126/science.1248364, 2014.

Chisholm, S.W.: Phytoplankton size, in: Primary productivity and biogeochemical cycles in the sea, edited by: Falkowski, P.G., and Woodhead A.D., Plenum, New York, 213-237, 1992.

Christian, J.: Biogeochemical cycling in the oligotrophic ocean: Redfield and non-Redfield models, Limnology and Oceanography, 50, 646-657, 2005.

https://doi.org/10.5194/gmd-2021-327
Preprint. Discussion started: 25 October 2021

Christian, J. and Karl, D.: Microbial community structure at the United States Joint Global Ocean Flux Study Station ALOHA - inverse methods for estimating biochemical indicator ratios, Journal of Geophysical Research-Oceans, 99, 14269-14276, 10.1029/94JC00681, 1994.

Christian, J., Arora, V., Boer, G., Curry, C., Zahariev, K., Denman, K., Flato, G., Lee, W., Merryfield, W., Roulet, N., and Scinocca, J.: The global carbon cycle in the Canadian Earth system model (CanESM1): Preindustrial control simulation, Journal of Geophysical Research-Biogeosciences, 115, 10.1029/2008JG000920, 2010.

Christian, J. R., Verschell, M. A., Murtugudde, R., Busalacchi, A. J., and McClain, C. R.: Biogeochemical modelling of the tropical Pacific Ocean. I: Seasonal and interannual variability, Deep-Sea Research Part II-Topical Studies in Oceanography, 49, 509-543, 2002a.

Christian, J. R., Verschell, M. A., Murtugudde, R., Busalacchi, A. J., and McClain, C. R.: Biogeochemical modelling of the tropical Pacific Ocean. II: Iron biogeochemistry, Deep-Sea Research Part II-Topical Studies in Oceanography, 49, 545-565, 0.1016/s0967-0645(01)00111-4, 2002b.

Denman, K. and Pena, M.: A coupled 1-D biological/physical model of the northeast subarctic Pacific Ocean with iron limitation, Deep-Sea Research Part II-Topical Studies in Oceanography, 46, 2877-2908, 10.1016/S0967-0645(99)00087-9, 1999.

Denman, K. and Pena, M.: The response of two coupled one-dimensional mixed layer/planktonic ecosystem models to climate change in the NE subarctic Pacific Ocean, Deep-Sea Research Part II-Topical Studies in Oceanography, 49, 5739-5757, 10.1016/S0967-0645(02)00212-6, 2002.

Denman, K., Voelker, C., Pena, M., and Rivkin, R.: Modelling the ecosystem response to iron fertilization in the subarctic NE Pacific: The influence of grazing, and Si and N cycling on CO_2 drawdown, Deep-Sea Research Part II-Topical Studies in Oceanography, 53, 2327-2352, 10.1016/j.dsr2.2006.05.026, 2006.

Devol, A.H.: Denitrification including anammox, in: Nitrogen in the Marine Environment, 2nd edition, edited by: Capone, D.G., Bronk D.A., Mulholland M.R., and Carpenter E.J., Elsevier, Amsterdam, 263-301, 2008.

Dickson, A.G., Sabine, C.L., and Christian, J.R., eds.: Guide to best practices for ocean CO_2 measurements, PICES Special Publication #3, 2007

Elser, J. and Urabe, J.: The stoichiometry of consumer-driven nutrient recycling: Theory, observations, and consequences, Ecology, 80, 735-751, 10.1890/0012-9658(1999)080[0735:TSOCDN]2.0.CO;2, 1999.

Franks, P., Wroblewski, J., and Flierl, G.: Behavior of a simple plankton model with food-level acclimation by herbivores, Marine Biology, 91, 121-129, 10.1007/BF00397577, 1986.

https://doi.org/10.5194/gmd-2021-327
Preprint. Discussion started: 25 October 2021

914 Friedlingstein, P., O'Sullivan, M., Jones, M., Andrew, R., Hauck, J., Olsen, A., Peters, G., Peters,
915 W., Pongratz, J., Sitch, S., Le Quere, C., Canadell, J., Ciais, P., Jackson, R., Alin, S., Aragao, L.,
916 Arneth, A., Arora, V., Bates, N., Becker, M., Benoit-Cattin, A., Bittig, H., Bopp, L., Bultan, S.,
917 Chandra, N., Chevallier, F., Chini, L., Evans, W., Florentie, L., Forster, P., Gasser, T., Gehlen,
918 M., Gilfillan, D., Gkritzalis, T., Gregor, L., Gruber, N., Harris, I., Hartung, K., Haverd, V.,
919 Houghton, R., Ilyina, T., Jain, A., Joetzjer, E., Kadono, K., Kato, E., Kitidis, V., Korsbakken, J.,
920 Landschutzer, P., Lefevre, N., Lenton, A., Lienert, S., Liu, Z., Lombardozzi, D., Marland, G.,
921 Metzl, N., Munro, D., Nabel, J., Nakaoka, S., Niwa, Y., O'Brien, K., Ono, T., Palmer, P., Pierrot,
922 D., Poulter, B., Resplandy, L., Robertson, E., Rodenbeck, C., Schwinger, J., Seferian, R.,
923 Skjelvan, I., Smith, A., Sutton, A., Tanhua, T., Tans, P., Tian, H., Tilbrook, B., Van der Werf,
924 G., Vuichard, N., Walker, A., Wanninkhof, R., Watson, A., Willis, D., Wiltshire, A., Yuan, W.,
925 Yue, X., and Zaehle, S.: Global Carbon Budget 2020, Earth System Science Data, 12, 3269-
926 3340, 10.5194/essd-12-3269-2020, 2020.
927
928 Friedrichs, M., Dusenberry, J., Anderson, L., Armstrong, R., Chai, F., Christian, J., Doney, S.,
929 Dunne, J., Fujii, M., Hood, R., McGillicuddy, D., Moore, J., Schartau, M., Spitz, Y., and
930 Wiggert, J.: Assessment of skill and portability in regional marine biogeochemical models: Role
931 of multiple planktonic groups, Journal of Geophysical Research-Oceans, 112,
932 10.1029/2006JC003852, 2007.
933
934 Garcia, H.E., Locarnini, R.A., Boyer, T.P., Antonov, J.I., Baranova, O.K., Zweng, M.M.,
935 Reagan, J.R., and Johnson, D.R.: World Ocean Atlas 2013, Volume 3: Dissolved Oxygen,
936 Apparent Oxygen Utilization, and Oxygen Saturation. S. Levitus, Ed., A. Mishonov Technical
937 Ed., NOAA Atlas NESDIS 75, 27 pp., 2014.
938
939 Garcia, H.E., Locarnini, R.A., Boyer, T.P., Antonov, J.I., Baranova, O.K., Zweng, M.M.,
940 Reagan, J.R., and Johnson, D.R.: World Ocean Atlas 2013, Volume 4: Dissolved Inorganic
941 Nutrients (phosphate, nitrate, silicate). S. Levitus, Ed., A. Mishonov Technical Ed.; NOAA Atlas
942 NESDIS 76, 25 pp., 2014.
943
944 Geider, R., MacIntyre, H., and Kana, T.: A dynamic regulatory model of phytoplanktonic
945 acclimation to light, nutrients, and temperature, Limnology and Oceanography, 43, 679-694,
946 1998.
947
948 Guilyardi, E. and Madec, G.: Performance of the OPA/ARPEGE-T21 global ocean-atmosphere
949 coupled model, Climate Dynamics, 13, 149-165, 10.1007/s003820050157, 1997.
950
951 Hayashida, H.: Modelling sea-ice and oceanic dimethylsulde production and emissions in the
952 Arctic, PhD thesis, University of Victoria, 2018.
953
954 Holdsworth, A.M., Zhai, L., Lu, Y., and Christian, J.R.: Future changes in oceanography and
955 biogeochemistry along the Canadian Pacific continental margin, Frontiers in Marine Science,
956 10.3389/fmars.2021.602991, 2021.
957
958 Jetten, M., Wagner, M., Fuerst, J., van Loosdrecht, M., Kuenen, G., and Strous, M.:
959 Microbiology and application of the anaerobic ammonium oxidation ('anammox') process,

https://doi.org/10.5194/gmd-2021-327
Preprint. Discussion started: 25 October 2021

960 Current Opinion in Biotechnology, 12, 283-288, 10.1016/S0958-1669(00)00211-1, 2001.
961
962 Johnson, K. S., Gordon, R. M., and Coale, K. H.: What controls dissolved iron concentrations in
963 the world ocean?, Marine Chemistry, 57, 137-161, 10.1016/s0304-4203(97)00043-1, 1997.
964
965 Johnson, K., Elrod, V., Fitzwater, S., Plant, J., Chavez, F., Tanner, S., Gordon, R., Westphal, D.,
966 Perry, K., Wu, J., and Karl, D.: Surface ocean-lower atmosphere interactions in the Northeast
967 Pacific Ocean Gyre: Aerosols, iron, and the ecosystem response, Global Biogeochemical Cycles,
968 17, 10.1029/2002GB002004, 2003.
969
970 Lambert, S. and Boer, G.: CMIP1 evaluation and intercomparison of coupled climate models,
971 Climate Dynamics, 17, 83-106, 10.1007/PL00013736, 2001.
972
973 Landry, M., Barber, R., Bidigare, R., Chai, F., Coale, K., Dam, H., Lewis, M., Lindley, S.,
974 McCarthy, J., Roman, M., Stoecker, D., Verity, P., and White, J.: Iron and grazing constraints on
975 primary production in the central equatorial Pacific: An EqPac synthesis, Limnology and
976 Oceanography, 42, 405-418, 10.4319/lo.1997.42.3.0405, 1997.
977
978 Lauvset, S., Key, R., Olsen, A., van Heuven, S., Velo, A., Lin, X., Schirnick, C., Kozyr, A.,
979 Tanhua, T., Hoppema, M., Jutterstrom, S., Steinfeldt, R., Jeansson, E., Ishii, M., Perez, F.,
980 Suzuki, T., and Watelet, S.: A new global interior ocean mapped climatology: the 1 degrees x 1
981 degrees GLODAP version 2, Earth System Science Data, 8, 325-340, 10.5194/essd-8-325-2016,
982 2016.
983
984 Li, Y.: Distribution patterns of the elements in the ocean - a synthesis, Geochimica et
985 Cosmochimica Acta, 55, 3223-3240, 1991.
986
987 Locarnini, R.A., Mishonov, A.V., Antonov, J.I., Boyer, T.P., Garcia, H.E., Baranova, O.K.,
988 Zweng, M.M., Paver, C.R., Reagan, J.R., Johnson, D.R., Hamilton, M., and Seidov, D.: World
989 Ocean Atlas 2013, Volume 1: Temperature. S. Levitus, Ed., A. Mishonov Technical Ed., NOAA
990 Atlas NESDIS 73, 40 pp., 2013.
991
992 Loladze, I., Kuang, Y., and Elser, J.: Stoichiometry in producer-grazer systems: Linking energy
993 flow with element cycling, Bulletin of Mathematical Biology, 62, 1137-1162,
994 10.1006/bulm.2000.0201, 2000.
995
996 Madec, G. and Imbard, M.: A global ocean mesh to overcome the North Pole singularity,
997 Climate Dynamics, 12, 381-388, 10.1007/s003820050115, 1996.
998
999 Moriarty, R. and O'Brien, T.: Distribution of mesozooplankton biomass in the global ocean,
1000 Earth System Science Data, 5, 45-55, 10.5194/essd-5-45-2013, 2013.
1001
1002 Nozaki, Y.: Elemental Distribution, in: Encyclopedia of Ocean Sciences, edited by: Steele, J.H.,
1003 Thorpe, S.A., and Turekian, K.K., Academic, San Diego, 840-845, 10.1006/rwos.2001.0402,
1004 2001.
1005

https://doi.org/10.5194/gmd-2021-327
Preprint. Discussion started: 25 October 2021

1006 Orr, J. C., Najjar, R. G., Aumont, O., Bopp, L., Bullister, J. L., Danabasoglu, G., Doney, S. C.,
1007 Dunne, J. P., Dutay, J. C., Graven, H., Griffies, S. M., John, J. G., Joos, F., Levin, I., Lindsay,
1008 K., Matear, R. J., McKinley, G. A., Mouchet, A., Oschlies, A., Romanou, A., Schlitzer, R.,
1009 Tagliabue, A., Tanhua, T., and Yool, A.: Biogeochemical protocols and diagnostics for the
1010 CMIP6 Ocean Model Intercomparison Project (OMIP), Geoscientific Model Development, 10,
1011 2169-2199, 10.5194/gmd-10-2169-2017, 2017.
1012
1013 Philander, S.G. and Chao, Y.: On the contrast between the seasonal cycles of the equatorial
1014 Atlantic and Pacific oceans, Journal of Physical Oceanography, 21, 1399-1406, 1991.
1015
1016 Raven, J. and Geider, R.: Temperature and algal growth, New Phytologist, 110, 441-461,
1017 10.1111/j.1469-8137.1988.tb00282.x, 1988.
1018
1019 Riche, O. and Christian, J.: Ocean dinitrogen fixation and its potential effects on ocean primary
1020 production in Earth system model simulations of anthropogenic warming, Elementa-Science of
1021 the Anthropocene, 6, 10.1525/elementa.277, 2018.
1022
1023 Schlitzer, R., Anderson, R., Dodas, E., Lohan, M., Geibere, W., Tagliabue, A., Bowie, A.,
1024 Jeandel, C., Maldonado, M., Landing, W., Cockwell, D., Abadie, C., Abouchami, W.,
1025 Achterberg, E., Agather, A., Aguliar-Islas, A., van Aken, H., Andersen, M., Archer, C., Auro,
1026 M., de Baar, H., Baars, O., Baker, A., Bakker, K., Basak, C., Baskaran, M., Bates, N., Bauch, D.,
1027 van Beek, P., Behrens, M., Black, E., Bluhm, K., Bopp, L., Bouman, H., Bowman, K., Bown, J.,
1028 Boyd, P., Boye, M., Boyle, E., Branellec, P., Bridgestock, L., Brissebrat, G., Browning, T.,
1029 Bruland, K., Brumsack, H., Brzezinski, M., Buck, C., Buck, K., Buesseler, K., Bull, A., Butler,
1030 E., Cai, P., Mor, P., Cardinal, D., Carlson, C., Carrasco, G., Casacuberta, N., Casciotti, K.,
1031 Castrillejo, M., Chamizo, E., Chance, R., Charette, M., Chaves, J., Cheng, H., Chever, F.,
1032 Christl, M., Church, T., Closset, I., Colman, A., Conway, T., Cossa, D., Croot, P., Cullen, J.,
1033 Cutter, G., Daniels, C., Dehairs, F., Deng, F., Dieu, H., Duggan, B., Dulaquais, G.,
1034 Dumousseaud, C., Echegoyen-Sanz, Y., Edwards, R., Ellwood, M., Fahrbach, E., Fitzsimmons,
1035 J., Flegal, A., Fleisher, M., van de Flierdt, T., Frank, M., Friedrich, J., Fripiat, F., Frollje, H.,
1036 Galer, S., Gamo, T., Ganeshram, R., Garcia-Orellana, J., Garcia-Solsona, E., Gault-Ringold, M.,
1037 George, E., Gerringa, L., Gilbert, M., Godoy, J., Goldstein, S., Gonzalez, S., Grissom, K.,
1038 Hammerschmidt, C., Hartman, A., Hassler, C., Hathorne, E., Hatta, M., Hawco, N., Hayes, C.,
1039 Heimburger, L., Helgoe, J., Heller, M., Henderson, G., Henderson, P., van Heuven, S., Ho, P.,
1040 Horner, T., Hsieh, Y., Huang, K., Humphreys, M., Isshiki, K., Jacquot, J., Janssen, D., Jenkins,
1041 W., John, S., Jones, E., Jones, J., Kadko, D., Kayser, R., Kenna, T., Khondoker, R., Kim, T.,
1042 Kipp, L., Klar, J., Klunder, M., Kretschmer, S., Kumamoto, Y., Laan, P., Labatut, M., Lacan, F.,
1043 Lam, P., Lambelet, M., Lamborg, C., Le Moigne, F., Le Roy, E., Lechtenfeld, O., Lee, J.,
1044 Lherminier, P., Little, S., Lopez-Lora, M., Lu, Y., Masque, P., Mawji, E., Mcclain, C., Measures,
1045 C., Mehic, S., Menzel Barraqueta, J., van der Merwe, P., Middag, R., Mieruch, S., Milne, A.,
1046 Minami, T., Moffett, J., Moncoiffe, G., Moore, W., Morris, P., Morton, P., Nakaguchi, Y.,
1047 Nakayama, N., Niedermiller, J., Nishioka, J., Nishiuchi, A., Noble, A., Obata, H., Ober, S.,
1048 Ohnemus, D., van Ooijen, J., O'Sullivan, J., Owens, S., Pahnke, K., Paul, M., Pavia, F., Pena, L.,
1049 Petersh, B., Planchon, F., Planquette, H., Pradoux, C., Puigcorbe, V., Quay, P., Queroue, F.,
1050 Radic, A., Rauschenberg, S., Rehkamper, M., Rember, R., Remenyi, T., Resing, J., Rickli, J.,
1051 Rigaud, S., Rijkenberg, M., Rintoul, S., Robinson, L., Roca-Marti, M., Rodellas, V., Roeske, T.,

https://doi.org/10.5194/gmd-2021-327
Preprint. Discussion started: 25 October 2021

1052 Rolison, J., Rosenberg, M., Roshan, S., van der Loaff, M., Ryabenko, E., Saito, M., Salt, L.,
1053 Sanial, V., Sarthou, G., Schallenberg, C., Schauer, U., Scher, H., Schlosser, C., Schnetger, B.,
1054 Scott, P., Sedwick, P., Semiletov, I., Shelley, R., Sherrell, R., Shiller, A., Sigman, D., Singh, S.,
1055 Slagter, H., Slater, E., Smethie, W., Snaith, H., Sohrin, Y., Sohst, B., Sonke, J., Speich, S.,
1056 Steinfeldt, R., Stewart, G., Stichel, T., Stirling, C., Stutsman, J., Swarr, G., Swift, J., Thomas, A.,
1057 Thorne, K., Till, C., Till, R., Townsend, A., Townsend, E., Tuerena, R., Twining, B., Vance, D.,
1058 Velazquez, S., Venchiarutti, C., Villa-Alfageme, M., Vivancos, S., Voelker, A., Wake, B.,
1059 Warner, M., Watson, R., van Weerlee, E., Weigand, M., Weinstein, Y., Weiss, D., Wisotzki, A.,
1060 Woodward, E., Wu, J., Wu, Y., Wuttig, K., Wyatt, N., Xiang, Y., Xie, R., Xue, Z., Yoshikawa,
1061 H., Zhang, J., Zhang, P., Zhao, Y., Zheng, L., Zheng, X., Zieringer, M., Zimmer, L., Ziveri, P.,
1062 Zunino, P., and Zurbrick, C.: The GEOTRACES Intermediate Data Product 2017, Chemical
1063 Geology, 493, 210-223, 10.1016/j.chemgeo.2018.05.040, 2018.
1064
1065 Séférian, R., Gehlen, M., Bopp, L., Resplandy, L., Orr, J., Marti, O., Dunne, J., Christian, J.,
1066 Doney, S., Ilyina, T., Lindsay, K., Halloran, P., Heinze, C., Segschneider, J., Tjiputra, J.,
1067 Aumont, O., and Romanou, A.: Inconsistent strategies to spin up models in CMIP5: implications
1068 for ocean biogeochemical model performance assessment, Geoscientific Model Development, 9,
1069 1827-1851, 10.5194/gmd-9-1827-2016, 2016.
1070
1071 Siegel, D., Buesseler, K., Behrenfeld, M., Benitez-Nelson, C., Boss, E., Brzezinski, M., Burd, A.,
1072 Carlson, C., D'Asaro, E., Doney, S., Perry, M., Stanley, R., and Steinberg, D.: Prediction of the
1073 Export and Fate of Global Ocean Net Primary Production: The EXPORTS Science Plan,
1074 Frontiers in Marine Science, 3, 10.3389/fmars.2016.00022, 2016.
1075
1076 Steinacher, M., Joos, F., Frolicher, T., Bopp, L., Cadule, P., Cocco, V., Doney, S., Gehlen, M.,
1077 Lindsay, K., Moore, J., Schneider, B., and Segschneider, J.: Projected 21st century decrease in
1078 marine productivity: a multi-model analysis, Biogeosciences, 7, 979-1005, 10.5194/bg-7-979-
1079 2010, 2010.
1080
1081 Stramski, D., Reynolds, R., Babin, M., Kaczmarek, S., Lewis, M., Rottgers, R., Sciandra, A.,
1082 Stramska, M., Twardowski, M., Franz, B., and Claustre, H.: Relationships between the surface
1083 concentration of particulate organic carbon and optical properties in the eastern South Pacific
1084 and eastern Atlantic Oceans, Biogeosciences, 5, 171-201, 10.5194/bg-5-171-2008, 2008.
1085
1086 Strous, M., Heijnen, J., Kuenen, J., and Jetten, M.: The sequencing batch reactor as a powerful
1087 tool for the study of slowly growing anaerobic ammonium-oxidizing microorganisms, Applied
1088 Microbiology and Biotechnology, 50, 589-596, 10.1007/s002530051340, 1998.
1089
1090 Swart, N., Cole, J., Kharin, V., Lazare, M., Scinocca, J., Gillett, N., Anstey, J., Arora, V.,
1091 Christian, J., Hanna, S., Jiao, Y., Lee, W., Majaess, F., Saenko, O., Seiler, C., Seinen, C., Shao,
1092 A., Sigmond, M., Solheim, L., von Salzen, K., Yang, D., and Winter, B.: The Canadian Earth
1093 System Model version 5 (CanESM5.0.3), Geoscientific Model Development, 12, 4823-4873,
1094 10.5194/gmd-12-4823-2019, 2019a.
1095
1096 Swart, N. C., Cole, J., Kharin, S., Lazare, M., Scinocca, J., Gillett, N., Anstey, J., Arora, V.,
1097 Christian, J., Hanna, S., Jiao, Y., Lee, W., Majaess, F., Saenko, O., Seiler, C., Seinen, C.,

https://doi.org/10.5194/gmd-2021-327
Preprint. Discussion started: 25 October 2021

1098 Shao, A., Solheim, L., von Salzen, K., Yang, D., and Winter, B.: The Canadian Earth System
1099 Model (CanESM), v5.0.3., https://doi.org/10.5281/zenodo.3251114, 2019b.
1100
1101 Takeda, S., Chai, F., and Nishioka, J., Eds.: Report of Working Group 22 on Iron Supply and its
1102 Impact on Biogeochemistry and Ecosystems in the North Pacific Ocean. PICES Sci. Rep. No.
1103 42, 60 pp., 2013.
1104
1105 Taylor, K.: Summarizing multiple aspects of model performance in a single diagram., Journal of
1106 Geophysical Research-Atmospheres, 106, 7183-7192, 10.1029/2000JD900719, 2001.
1107
1108 Tesdal, J., Christian, J., Monahan, A., and von Salzen, K.: Evaluation of diverse approaches for
1109 estimating sea-surface DMS concentration and air-sea exchange at global scale, Environmental
1110 Chemistry, 13, 390-412, 10.1071/EN14255, 2016.
1111
1112 von Salzen, K., Scinocca, J. F., McFarlane, N. A., Li, J. N., Cole, J. N. S., Plummer, D.,
1113 Verseghy, D., Reader, M. C., Ma, X. Y., Lazare, M., and Solheim, L.: The Canadian Fourth
1114 Generation Atmospheric Global Climate Model (CanAM4). Part I: Representation of Physical
1115 Processes, Atmosphere-Ocean, 51, 104-125, 10.1080/07055900.2012.755610, 2013.
1116
1117 White, J., Zhang, X., Welling, L., Roman, M., And Dam, H.: Latitudinal gradients in
1118 zooplankton biomass in the tropical Pacific At 140°W During The JGOFS Eqpac study - effects
1119 of El Nino, Deep-Sea Research Part II-Topical Studies in Oceanography, 42, 715-733,
1120 10.1016/0967-0645(95)00033-M, 1995.
1121
1122 Wolf-Gladrow, D., Zeebe, R., Klaas, C., Kortzinger, A., and Dickson, A.: Total alkalinity: The
1123 explicit conservative expression and its application to biogeochemical processes, Marine
1124 Chemistry, 106, 287-300, 10.1016/j.marchem.2007.01.006, 2007.
1125
1126 Zahariev, K., Christian, J., and Denman, K.: Preindustrial, historical, and fertilization simulations
1127 using a global ocean carbon model with new parameterizations of iron limitation, calcification,
1128 and N_2 fixation, Progress in Oceanography, 77, 56-82, 10.1016/j.pocean.2008.01.007, 2008.
1129
1130 Zweng, M.M., Reagan, J.R., Antonov, J.I., Locarnini, R.A., Mishonov, A.V., Boyer, T.P.,
1131 Garcia, H.E., Baranova, O.K., Johnson, D.R., Seidov, D., and Biddle, M.M.: World Ocean Atlas
1132 2013, Volume 2: Salinity. S. Levitus, Ed.; A. Mishonov, Technical Ed., NOAA Atlas NESDIS
1133 74, 39 pp., 2013.
1134